Earth-Science Reviews 226 (2022) 103944

Contents lists available at ScienceDirect

Earth-Science Reviews

journal homepage: www.elsevier.com/locate/earscirev

Land-surface parameters for spatial predictive mapping and modeling

Aaron E. Maxwell *, Charles M. Shobe

Department of Geology and Geography, West Virginia University, Morgantown, WV USA

ARTICLE INFO

Keywords:
Geomorphometry
Land-surface parameters
Digital land surface model
Digital elevation model
Landforms
Spatial predictive modeling
machine learning

ABSTRACT

Land-surface parameters derived from digital land surface models (DLSMs) (for example, slope, surface curvature, topographic position, topographic roughness, aspect, heat load index, and topographic moisture index) can serve as key predictor variables in a wide variety of mapping and modeling tasks relating to geomorphic processes, landform delineation, ecological and habitat characterization, and geohazard, soil, wetland, and general thematic mapping and modeling. However, selecting features from the large number of potential derivatives that may be predictive for a specific feature or process can be complicated, and existing literature may offer contradictory or incomplete guidance. The availability of multiple data sources and the need to define moving window shapes, sizes, and cell weightings further complicate selecting and optimizing the feature space. This review focuses on the calculation and use of DLSM parameters for empirical spatial predictive modeling applications, which rely on training data and explanatory variables to make predictions of landscape features and processes over a defined geographic extent. The target audience for this review is researchers and analysts undertaking predictive modeling tasks that make use of the most widely used terrain variables.

To outline best practices and highlight future research needs, we review a range of land-surface parameters relating to steepness, local relief, rugosity, slope orientation, solar insolation, and moisture and characterize their relationship to geomorphic processes. We then discuss important considerations when selecting such parameters for predictive mapping and modeling tasks to assist analysts in answering two critical questions: What landscape conditions or processes does a given measure characterize? How might a particular metric relate to the phenomenon or features being mapped, modeled, or studied? We recommend the use of landscape- and problem-specific pilot studies to answer, to the extent possible, these questions for potential features of interest in a mapping or modeling task. We describe existing techniques to reduce the size of the feature space using feature selection and feature reduction methods, assess the importance or contribution of specific metrics, and parameterize moving windows or characterize the landscape at varying scales using alternative methods while highlighting strengths, drawbacks, and knowledge gaps for specific techniques. Recent developments, such as explainable machine learning and convolutional neural network (CNN)-based deep learning, may guide and/or minimize the need for feature space engineering and ease the use of DLSMs in predictive modeling tasks.

1. Introduction

Land-surface parameters, or geomorphometric variables, can be important indicators or predictor variables for a wide variety of spatial predictive modeling and thematic mapping tasks (Ironside et al., 2018; Florinsky, 2017; Franklin, 2020). For example, such variables have been documented to be of value for mapping or predicting landforms (e.g., Cavalli et al., 2017; Clubb et al., 2014; McKean and Roering, 2004; Purinton and Bookhagen, 2017; Sofia, 2020), geomorphic processes (e.g., Drăguţ and Blaschke, 2006; Eisank et al., 2011; Gerçek et al., 2011; Maxwell et al., 2020b), geohazards (e.g., Brock et al., 2020; Goetz et al., 2015; Maxwell et al., 2020c, 2021), soil properties (e.g., Florinsky et al., 2002; Gesseler et al., 1995; Vermeulen and Van Niekerk, 2017), ecological and habitat characteristics (e.g., Ironside et al., 2018; Evans and Cushman, 2009), and wetland extent (e.g., Maxwell et al., 2016; Maxwell and Warner, 2019a, 2019b; Riley et al., 2017; Wright and Gallant, 2007). The development of consistent, detailed, and publicly available digital land surface models (DLSMs), such as those being curated by the 3D Elevation Program (3DEP) (Arundel et al., 2015) in the United States (USA), has greatly increased the availability of data for undertaking operational mapping and modeling tasks over large spatial extents (Csillik and Drăguţ, 2018; Franklin, 1987; Guth, 2006; Höfle and

* Corresponding author.
E-mail addresses: Aaron.Maxwell@mail.wvu.edu (A.E. Maxwell), Charles.Shobe@mail.wvu.edu (C.M. Shobe).

https://doi.org/10.1016/j.earscirev.2022.103944
Received 7 September 2021; Received in revised form 18 January 2022; Accepted 24 January 2022
Available online 29 January 2022

Rutzinger, 2011; James et al., 2012). Data have been and continue to be generated at a variety of spatial resolutions and levels of generalization or detail; for example, the Shuttle Radar Topography Mission (SRTM) digital elevation model (DEM), which covers 80% of the globe between 60° north and 56° south, offers spatial resolutions of one arc-second (roughly 30-by-30 m pixels) and three arc-seconds (roughly 90-by-90 m pixels) (Farr et al., 2007). Similarly, the Advanced Spaceborne Thermal Emission and Reflection Radiometer Global Digital Elevation Model (ASTER Global Digital Elevation Map, 2021) offers a 30 m spatial resolution ("ASTER Global Digital Elevation Map"). In contrast, light detection and ranging (LiDAR) can offer a high (i.e., sub-meter) spatial resolution along with the ability to map features below tree canopies using multiple returns from a single laser pulse (Höfle and Rutzinger, 2011). The availability of DLSM datasets representing landscapes at different times can support the quantification of landscape change resulting from anthropogenic alterations and natural geomorphic processes (James et al., 2012; Maxwell and Strager, 2013; Perignon et al., 2013; Ross et al., 2016; Williams, 2012; Yang et al., 2021).

Despite the demonstrated utility of DLSMs and derived land-surface parameters, making use of these data for specific mapping or modeling tasks is complex. First, the analyst must select a DLSM source. Fine spatial resolution or detail may enhance the visibility of desired features but can also be unnecessary or even a hindrance. Second, a wide variety of parameters can be generated such that determining a reasonable or suitable variable subset, or feature space, for a specific task can be difficult. Prior research may offer inadequate or contradictory guidance (see for example Franklin (2020) and Maxwell et al. (2020a, 2020b, 2020c)), and a suitable subset of features is commonly not known *a priori*, requiring the analyst to investigate a large number of inputs or develop a feature set that may be suboptimal. Such experimentation can be time consuming and computationally intensive. Third, many land-surface parameters may be highly correlated, which can cause problems when used as input for algorithms or modeling methods that are not robust to multicollinearity. Fourth, many parameters make use of local moving windows or kernels that compare a center cell to its neighbors. For such variables, the analyst may struggle to specify an appropriate window shape and size, be unsure of whether the cells in the window should be weighted based on distance from the center cell, and be faced with a wide array of weighting options if weighting appears to be warranted. Alternatively, analysts may explore other means to characterize the landscape at multiple scales that do not rely on traditional moving window-based analysis (e.g., resampling DLSMs to a coarser spatial resolution or smoothing the surface using a filter). Lastly, due to issues of spatial heterogeneity, relationships and patterns may not be consistent across landscapes or physiographies. Given the richness of available options and, in many cases, the lack of guidance provided by prior research, variable selection and generation can be a daunting task (Albani et al., 2004; Ironside et al., 2018; Evans and Minár, 2011; Florinsky, 2017; Franklin, 1987, 2020; Hengl et al., 2009; MacMillan and Shary, 2009; Olaya and Conrad, 2009; Pike et al., 2009; Wilson and Gallant, 2000).

Prior studies—and two key texts—provide reviews of land-surface parameters and their uses. Chapters 3 and 4 in Wilson and Gallant's *Terrain Analysis: Principles and Applications* text (Wilson and Gallant, 2000) explain and review a wide range of parameters. Hengl and Reuter (2009) *Geomorphometry: Concepts, Software, and Applications* provides a detailed treatment of geomorphometry, with Chapters 6 through 8 focused on land-surface parameters specifically (Hengl and Reuter, 2009). Florinsky (2017) provides a mathematical treatment, categorization, and review of a wide range of geomorphometric methods and metrics in order to foster a deeper understanding of their meaning and correct use. Ironside et al. (2018) review the use of land-surface parameters in ecological applications and highlight that the optimal subset of variables is often case- and/or landscape-specific. Franklin (2020) explores the use of these parameters in geophysical and biophysical remote sensing studies and highlights the need to select features based on a clear conceptualization of how each variable may influence the phenomenon being studied or predicted and why its inclusion is likely beneficial. Sofia (2020) reviews the use of geomorphometry for deriving insight into Earth surface process dynamics through both direct analysis of parameters and their use in empirical models. Xiong et al. (2021) argue for a shift in focus from mapping and quantifying landscape characterisitics to using DLSMs and analytical techniques to model the mechanisms that generate landforms and further our understanding of geomorphic processes. Whether the goal is mapping a landscape property or generating mechanistic insight, both require the judicious use of parameters derived from DLSMs.

Expanding upon prior studies and reviews, we focus on how to select and use land-surface parameters as inputs to empirical spatial predictive mapping and modeling tasks, including geomorphic mapping and modeling, spatial probabilistic modeling, and thematic mapping or landscape classification tasks such as vegetation or forest type differentiation, wetland delineation, and land use/land cover (LULC) data production. In contrast to other recent geomorphometry-relevant reviews (e.g., Florinsky, 2017; Ironside et al., 2018; Franklin, 2020; Sofia, 2020; and Xiong et al., 2021), we focus on parameterization issues specific to empirical modeling tasks including selecting input elevation data, impacts of data generalization and spatial resolution on calculated metrics and resulting models, parameterization of moving windows, alternative means to characterize landscapes at multiple scales, and feature selection and reduction. This review is of specific value to those with a need to characterize the landscape to undertake empirical modeling tasks, especially in cases where *a priori* knowledge of the most important land-surface parameters for a given task is not available.

Empirical modeling relies on samples, or training data, and explanatory variables to make predictions of continuous measures (regression), differentiate categories (classification), or estimate probabilities (probabilistic predictive modeling). Commonly employed techniques include linear and multiple linear regression, geographically weighted regression, logistic regression, generalized additive models (GAMs), machine learning (e.g., artificial neural networks (ANN), support vector machines (SVM), decision trees (DT), random forest (RF), and boosted DTs), and deep learning. For spatial predictive modeling specifically, the output will be predictions over a map extent relative to some aggregating unit, such as pixels/cells or areal features (Chang, 2008; James et al., 2013; Lillesand et al., 2015; Maxwell et al., 2018).

Based on results from prior studies, we highlight best practices and suggest future research needs. In Section 2 (Digital Land Surface Models and Derived Parameters), we provide an overview of DLSMs and the types of land-surface parameters that can be derived from them. In Section 3 (Considerations for Calculating, Selecting, and Implementing Land-Surface Parameters for Empirical Modeling), we discuss selecting variables, means of feature selection or reduction, issues of scale and spatial resolution, defining and parameterizing moving windows, alternatives to moving windows, and comparing multiple DEMs to assess landscape change. In Section 4 (Recommendations and Research Needs), we summarize best practices and highlight knowledge gaps.

2. Digital land surface models and derived parameters

2.1. Digital land surface models

A digital representation of the bare-earth surface elevation is commonly called a digital terrain model (DTM). In contrast, a surface that includes aboveground features, such as trees and buildings, is referred to as a digital surface model (DSM). The term digital elevation model (DEM) is more generic and can be used to refer to a DTM or a DSM. In this review, we use the term digital land surface model (DLSM), as opposed to DTM, to denote a representation of the bare-earth surface as suggested by Pike et al. (2009), as this is the preferred term within the geomorphometry community (Pike et al., 2009; Hengl and Reuter, 2009). In order to estimate the height of features above the landscape

surface, a DLSM can be subtracted from a DSM to obtain a normalized digital surface model (nDSM), in which the measurements represent height above the ground surface. If only trees or forest canopy are represented as aboveground features, an nDSM may be referred to as a canopy height model (CHM) (Chang, 2008; Wilson and Gallant, 2000). DLSMs of difference are produced by subtracting two DLSMs representing different time periods and provide a measure of elevation loss or gain at each cell (Williams, 2012).

Elevation data can be represented as discrete point measurements, isolines or contour lines, or continuous surfaces. The triangulated irregular network (TIN) vector-based model allows for measurements at discrete data points to be interpolated to a continuous surface using a triangular mesh, where each triangular facet is defined by the three point measurements that form its vertices. However, most analytical methods for generating land-surface parameters rely on a raster-based data model where each cell has a defined size (e.g., 10-by-10 m) and holds an elevation measurement. What the elevation measurement represents for each cell is not always clear; for example, the elevation could represent an average over the cell or the elevation at the center of the cell, which could impact the interpretation and use of the surface (Chang, 2008). Here, we will make use of this raster-based representation of terrain surfaces. Raster data models can be augmented to represent vectors (i.e., quantities that have both magnitude and direction) as opposed to scalar quantities. This augmentation of the raster data model is known as vector fields and allows for vector algebra and calculus to be implemented to calculate land-surface parameters (Li and Hodgson, 2004; Hu et al., 2021a, 2021b). For example, Hu et al. (2021a, 2021b) proposed a method for calculating plan curvatures using vector fields. Raster-based vectors are also implicitly used in dynamical landscape evolution models in which the divergence of sediment fluxes between raster cells governs topographic change (e.g., Tucker and Hancock, 2010).

A variety of methods are available to estimate the elevation of the landscape surface and generate DLSMs and/or DSMs. The traditional

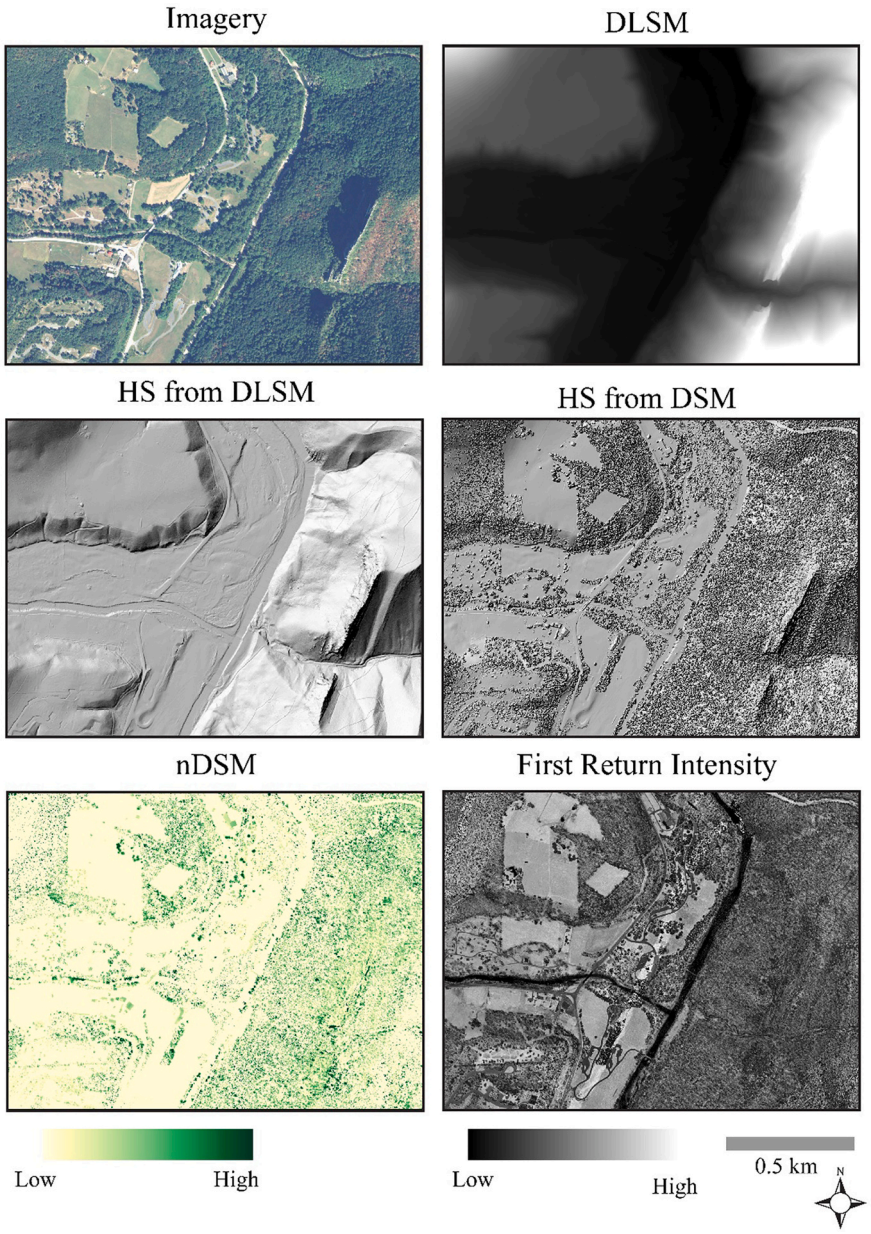

Fig. 1. Example variables derived from LiDAR data. Image data are provided for comparison and are from the National Agriculture Imagery Program (NAIP). DLSM = Digital Land Surface Model, DSM = Digital Surface Model, nDSM = normalized Digital Surface Model. The DLSM and DSM are visualized using a hillshade (HS). All LiDAR derivatives were generated using ArcGIS Pro (ArcGIS Pro help—ArcGIS Pro | Documentation, 2021).

approach uses passive remote sensing and photogrammetry that exploits the stereo parallax in overlapping stereo images to estimate heights. This same general approach is used in the creation of DSMs using many overlapping drone images, a process known as structure from motion (SfM). Active remote sensing methods used to generate elevation datasets include interferometric synthetic aperture radar (InSAR), which makes use of differences in phase between returning backscatter waveforms, and LiDAR, which uses laser range distancing to produce point clouds representing *x*, *y*, *z* coordinates in three-dimensional space. Since many systems can also record multiple returns from a single laser pulse, returns from subcanopy features—and even the ground surface—can potentially be recorded, allowing for the mapping of geomorphic features and terrain surfaces otherwise obscured by vegetation. Traditional photogrammetry, SfM, and InSAR do not allow for canopy penetration, which hinders the production of DLSMs in forested areas (Chang, 2008; Höfle and Rutzinger, 2011; Lillesand et al., 2015).

Fig. 1 demonstrates the quality and variety of information that can be obtained from multiple-return aerial LiDAR. Our examples use LiDAR data for an area near Seneca Rocks in West Virginia, USA. For comparison, in Fig. 1 we have also included an aerial orthophotograph provided by the National Agriculture Imagery Program (NAIP). The DLSM, visualized here using a hillshade, highlights the detail of the bare-earth surface captured. The DSM, also displayed as a hillshade, highlights the generally rough nature of the vegetation surface compared to the generally much smoother bare earth. The nDSM represents heights above ground while the spectral information associated with the intensity of the near infrared laser returns is visualized using a first return intensity image, which has some correlation with land cover and surface materials (Lillesand et al., 2015).

2.2. Land-surface parameters

In this section, we review the most commonly used land-surface parameters that can be calculated from DLSMs. As noted above, there are a wide variety of surfaces that can be generated (Wilson and Gallant, 2000); it is not possible to provide a detailed treatment of all possible features. We focus on selected metrics that explain or quantify key aspects of the land surface such as steepness, local relief, rugosity, slope orientation, solar insolation, and moisture. While this overview focuses on the most commonly used metrics that quantify different aspects of the land surface, our later discussion of feature selection and reduction methods is applicable to a much broader range of land-surface parameters.

2.2.1. Visualizing bare-earth surfaces

Creating effective visualizations of DLSMs is critical for allowing both intuitive user understanding of the data (Roering et al., 2013) and effective modeling (Maxwell et al., 2020b). Multiple methods exist for visualizing DLSMs (Fig. 2). A hillshade (HS) represents illumination of a terrain surface; the illumination of a given cell depends on the position of the illuminating source and the terrain steepness and orientation at the cell location. In order to potentially improve the visualization of the landscape for all slopes, regardless of the compass direction at which they are oriented, a multidirectional hillshade (MDHS) can be calculated through averaging, or weighted averaging, of multiple HSs generated using different illuminating geometries. Visualization of the DLSM may be further improved by using transparency and combining a HS or MDHS with a color ramp representing elevation measurements, a surface known as a hypsometrically-tinted hillshade (HTHS). It is also possible to include measures of surface curvature or topographic position, both discussed below, to further differentiate or highlight ridges and valleys. Contour lines can be included to further improve

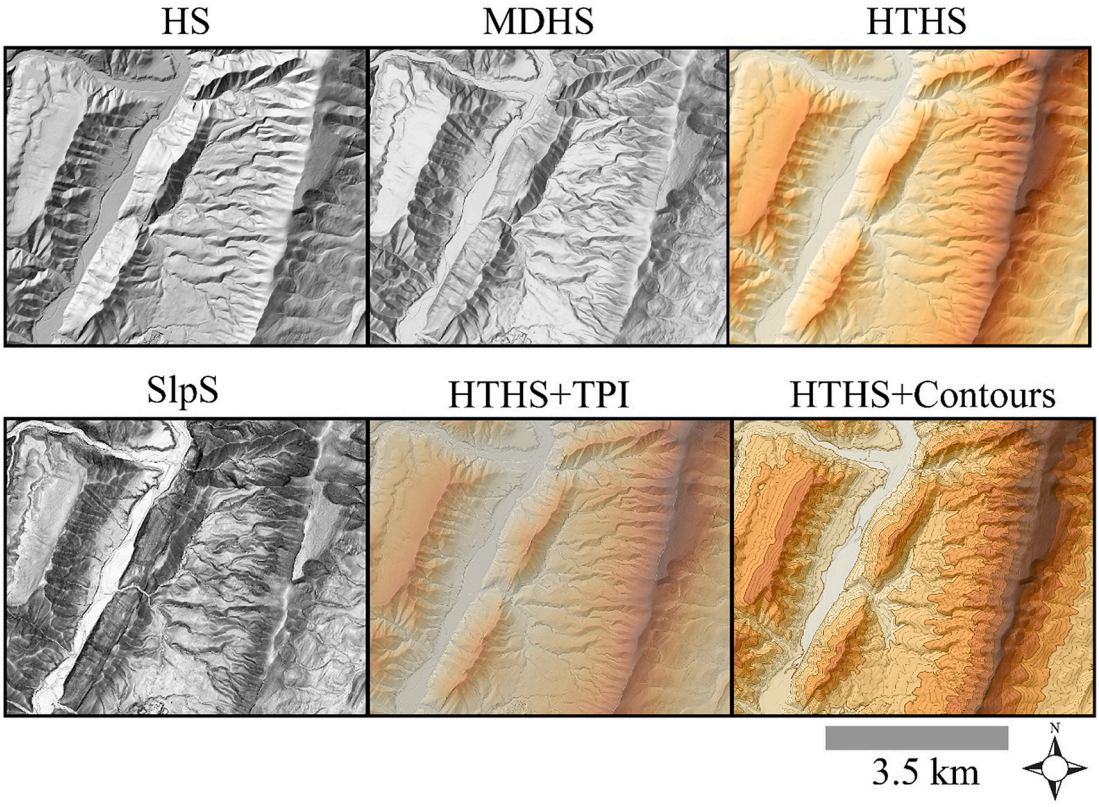

Fig. 2. Example terrain visualizations for manual interpretation. HS = hillshade, MDHS = multi-directional hillshade, HTHS = hypsometrically-tinted hillshade, SlpS = Slopeshade, HTHS+TPI = hypsometrically-tinted hillshade plus topographic position index (TPI), HTHS+Contours = hypsometrically-tinted hillshade plus contours. All visualizations were created using ArcGIS Pro (ArcGIS Pro help—ArcGIS Pro | Documentation, 2021).

interpretability (Brewer, 2005; Chang, 2008; Howard et al., 2008).

As an alternative to HS-based DLSM visualizations, a slopeshade (SlpS) can be calculated from a topographic slope surface (Fig. 2), which is discussed below. To create a SlpS, a topographic slope raster grid is symbolized using a light-to-dark color ramp where lighter shades represent flatter terrain and darker shades represent steeper surfaces. SlpSs do not require defining the position of an illuminating source and are illumination-invariant (Doctor and Young, 2013; Maxwell et al., 2020b; Reed and Kite, 2020).

2.2.2. Topographic slope

Fig. 3 shows some common land-surface parameters that can be calculated from DLSMs. One of the most common derivatives is an estimate of the local topographic steepness or slope (Slp) (Eq. (1)). Slope is a simple yet critical terrain variable, as it is often a key predictor of landslides and other geohazards that spatial modeling seeks to map and predict (Maxwell et al., 2020c, 2021; Stanley and Kirschbaum, 2017). Slope is also key from a geomorphic perspective. Sediment transport and erosion rates on hillslopes and in river channels typically increase at least linearly with slope (Andrews and Bucknam, 1987; Lague et al., 2003; Lague and Davy, 2003); the relationship between slope and upslope drainage area is the fundamental determinant of geomorphic process across most landscapes (Montgomery and Dietrich, 1992; Tucker and Bras, 1998; Willgoose et al., 1991).

$$\text{Slp (radians)} = arctan\left(\sqrt{\left(\frac{\partial z}{\partial x}\right)^2 + \left(\frac{\partial z}{\partial y}\right)^2}\right) \quad (1)$$

As the 1st derivative of the elevation surface, slope is commonly calculated using elevation values in a 3-by-3 cell window, bivariate quadratic equations, or the partial differential of elevation relative to the x and y planes (Eq. (1)). Mean slope (MnSlp) is an average slope produced by calculating the mean slope from a Slp grid within moving windows to obtain a smoother representation of steepness.

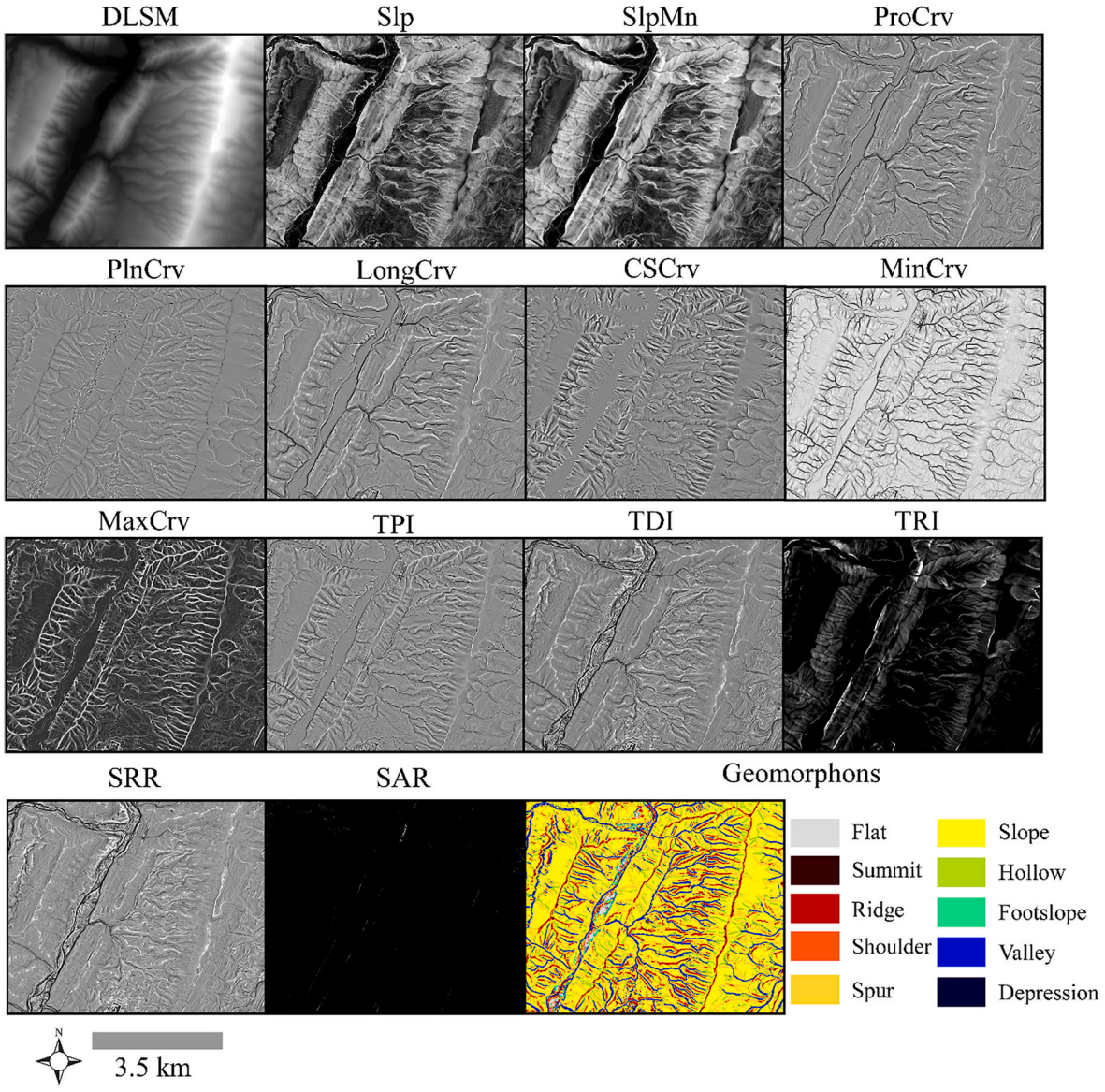

Fig. 3. Example metrics that characterize local relief, terrain shape, and landforms. DLSM = digital land surface model, Slp = topographic slope, SlpMn = mean topographic slope, ProCrv = profile curvature, PlnCrv = plan curvature, LongCrv = longitudinal curvature, CSCrv = cross-sectional curvature, MinCrv = minimum curvature, MaxCrv = maximum curvature, TPI = topographic position index, TDI = topographic dissection index, TRI = topographic roughness index, SRR = surface relief ratio, and SAR = surface area ratio. Surface curvatures, TPI, and geomorphons were calculated using SAGA (Olaya and Conrad, 2009). Slp was calculated using ArcGIS Pro (ArcGIS Pro help—ArcGIS Pro | Documentation, 2021) while all other measures were calculated using R (R Core Team, 2020) and the spatialEco package (Evans, 2020).

Alternatively, slope can be calculated using a larger window, which leads to a similar generalization (Chang, 2008; Wilson and Gallant, 2000).

2.2.3. Surface curvature

Surface or topographic curvature (Crv) generally relates to the shape of the local land surface with respect to terrain convexity or concavity. Curvature describes the convergent or divergent nature of the topographic surface, thereby providing an important indicator of dominant geomorphic processes (Hooshyar and Wang, 2016; Tarolli et al., 2012), landscape hydrology (Bogaart and Troch, 2006; Heerdegen and Beran, 1982), and soil properties (Gesseler et al., 1995). Curvature can reflect rates of soil production and erosion (Dietrich et al., 1995; Heimsath et al., 1997; Thaler et al., 2021). Hilltop curvature, for example, is correlated with the hilltop erosion rate such that "sharper" ridgetops reflect more rapid erosion (Gabet et al., 2021; Hurst et al., 2013; Struble et al., 2021).

Curvature is the 2nd derivative of elevation and relates to the deviation of a terrain line from being straight or a terrain surface from being flat (Guth, 2009; Hofierka et al., 2009; Minár et al., 2020; Minár et al., 2013; Wood, 2009; Wood, 1996; Zevenbergen and Thorne, 1987). Curvature calculations are complicated as different measures can be obtained based on how curvature is defined relative to the direction of maximum slope. Most calculations rely on fitting polynomials (Ehsani and Quiel, 2008; Evans, 1972; Hurst et al., 2012; Minár et al., 2020; Roering et al., 1999; Tarolli et al., 2012; Wilson et al., 2007). However, other methods are available. For example, Struble and Roering (2021) proposed a method based on continuous wavelet transforms. Additional complexity stems from the fact that many measures of curvature have been defined with different names used to represent the same measure, the same name used to define different measures, variability or even errors in how measures are calculated, and poorly documented calculation methods (Minár et al., 2020). Many of these curvatures are heavily correlated, as is evident in the examples in Fig. 3. There also exist disconnects between theory and application. For example, the curvature measures used in studies and operational projects are often dictated by the software environment(s) available as opposed to correlation with the phenomenon being investigated, mapped, or modeled (Guth, 2009; Hofierka et al., 2009; Minár et al., 2020, Minár et al., 2013; Wood, 2009, Wood, 1996; Zevenbergen and Thorne, 1987).

Minár et al. (2020) provide a review, critique, and systemization of curvature measures. They suggest that curvature measures can be grouped into three broad categories based on similar interpretations of convex and concave landforms: plan, profile, and twisting. Generally, plan curvatures, such as normal contour or plan curvature, are calculated in the direction of minimum gravitational potential energy, or perpendicular to the direction of maximum slope. Profile curvatures, such as normal slope line or profile curvature, are calculated in the direction of maximum slope. Twisting curvatures, such as rotor curvature, relate to local "twisting" of the terrain surface and are calculated relative to a direction neither parallel to nor perpendicular to the direction of maximum slope. Twisting curvatures are mixed second derivatives of elevation and relate to changes in the aspect or direction of maximum slope, but unlike plan and profile curvature are relatively poorly understood and demonstrate uncertain utility in the context of geomorphometric analysis, spatial mapping, and modeling. Other curvature measures are combinations of the three basic types (Minár et al., 2020).

This highlights the complexity of choosing curvature measures for specific tasks. Minár et al. (2020) summarize typical uses and synthesize how landforms or surface processes may be reflected in specific curvature measures. We suggest that this source be consulted for choosing a subset of curvature measures.

2.2.4. Topographic position and variability

The topographic position index (TPI) serves as a measure of local or hillslope-scale topographic position (Wilson and Gallant, 2000). TPI is calculated by subtracting the mean of all elevation measurements within a moving window (z_{mean}) from the center cell elevation (z) (Eq. (2)). Larger, positive values indicate higher topographic positions (e.g., ridges) while larger, negative values indicate lower positions (e.g., valleys) (De Reu et al., 2013; Hengl et al., 2009; Lopez and Berry, 2002; MacMillan and Shary, 2009; Riley et al., 2017; Wilson and Gallant, 2000).

$$\mathrm{TPI} = z - z_{mean} \tag{2}$$

The topographic roughness index (TRI) represents the variance (σ^2) in elevation measurements (z) within a local window (Eq. (3)). Terrain roughness can be indicative of landscape-scale underlying geologic conditions (Kreslavsky et al., 2013), geomorphic process dominance (Milodowski et al., 2015), and the cumulative influence of surface processes over time (Johnstone et al., 2018; LaHusen et al., 2016). Higher values indicate higher local rugosity, or a more rugged or variable terrain surface (Blaszczynski, 1997; Hengl et al., 2009; MacMillan and Shary, 2009; Riley et al., 1999; Wilson and Gallant, 2000). Surface relief ratio (SRR) offers another measure of rugosity (Eq. (4)) (MacMillan and Shary, 2009; Pike et al., 2009; Pike and Wilson, 1971; Wilson and Gallant, 2000). SRR—which is equivalent to the hypsometric integral (Pike and Wilson, 1971)—can roughly indicate the state of relief in an area and may therefore correlate with lithologic or tectonic boundary conditions (Chen et al., 2003; Lifton and Chase, 1992). Surface area ratio (SAR) (Eq. (5)) is the ratio of the estimated landscape surface area to the planar area at a cell location (Jenness, 2004).

$$\mathrm{TRI} = \sigma^2(z) \tag{3}$$

$$\mathrm{SRR} = \frac{z_{\mathrm{mean}} - z_{\mathrm{min}}}{z_{\mathrm{max}} - z_{\mathrm{min}}} \tag{4}$$

$$\mathrm{SAR} = \frac{\mathrm{Cell\ Size}^2}{\mathrm{Cos(Slope\ in\ Degrees)}} \tag{5}$$

The topographic dissection index (TDI) (Eq. (6)) is a measure of how high above the bottom of a landscape a given point sits, which may be related to incision such as by channels. Lower values indicate more incision (Evans, 1972; MacMillan and Shary, 2009; Wilson and Gallant, 2000).

$$\mathrm{TDI} = \frac{z - z_{min}}{z_{max} - z_{min}} \tag{6}$$

Metrics derived from the gray level co-occurrence matrix (GLCM) after Haralick et al. (1973) provide another means to generate local textural measures from raster datasets. The GLCM is a table of the frequency within a local window of the occurrence of all combinations of elevations for neighboring pixels. Neighboring pixels are defined as two locations at a specified offset (distance apart) and direction, though it is common to average multiple directions. Because the GLCM table has *N*-by-*N* entries, where *N* is the number of possible elevation values in the DLSM, it is useful to limit the table size by re-scaling the elevations to a limited range of possible values. Once the table has been generated for a pixel and its local window, a variety of derived metrics can be calculated (Table 1). The measures can be grouped into three categories as measures of contrast, orderliness, and descriptive statistics (Hall-Beyer, 2017; Warner, 2011). Hall-Beyer (2017) suggests including one measure of contrast, one measure of orderliness, and two to three descriptive statistics to summarize the GLCM.

The application of GLCM textures to DLSMs has been explored by numerous authors. For example, Kai et al. (2013) assessed the use of GLCM-based, DLSM-derived textural measures for landform classification and noted the value of the measures. Zhao et al. (2017) incorporated these measures into a geographic object-based image analysis (GEOBIA) framework for extracting terraces within the Loess Plateau in China.

Table 1
Example texture measures calculated from the gray level co-occurrence matrix (GLCM).

Group	Variable	Description
Contrast	Contrast	$\sum_{i,j=0}^{N-1} p_{ij}(i-j)^2$
	Dissimilarity	$\sum_{i,j=0}^{N-1} p_{ij}\lvert i-j\rvert$
	Homogeneity	$\sum_{i,j=0}^{N-1} \frac{p_{ij}}{1+(i-j)^2}$
Orderliness	Angular Second Moment	$\sum_{i,j=0}^{N-1} p_{ij}^2$
	Entropy	$\sum_{i,j=0}^{N-1} p_{ij}(-ln(p_{ij}))$
Descriptive Statistics	Mean	$\sum_{i,j=0}^{N-1} i(p_{ij})\mu_j; \sum_{i,j=0}^{N-1} i(p_{ij})$
	Variance	$\sum_{i,j=0}^{N-1} p_{ij}(i-\mu_i)^2$; $\sum_{i,j=0}^{N-1} p_{ij}(j-\mu_j)^2 \sigma_i$
	Correlation	$\sum_{i,j=0}^{N-1} p_{ij}\left((i-\mu_i)(i-\mu_j)\right)/\sqrt{\sigma_i^2\sigma_j^2}$

i = GLCM row number; j = GLCM column number; $p_{i,j}$ = probability of (rescaled) elevation values i and j being neighbors at the specified offset and direction; N = number of rows (also the number of columns and the maximum number of potential values the rescaled elevation values can take on); μ = mean, σ^2 = variance.

2.2.5. Geomorphons

The variables discussed above provide continuous measures or indices of landscape characteristics. In contrast, geomorphologic phenotypes, or geomorphons (Fig. 3), represent a categorization of terrain features or landform types that are size-, orientation-, and local relief-invariant. A cell is compared to its neighbors in eight directions to characterize the patterns on the landscape and determine in which directions elevation is higher, lower, or at the same altitude as the reference cell location. So as not to limit the analysis to a 3-by-3 cell window and to allow for mapping similar landforms with variable sizes or scales, a line-of-sight method is used as opposed to the direct cell neighbors. A total of 498 patterns are categorized, which can then be subsequently grouped into common terrain features or landforms (Stepinski and Jasiewicz, 2011; Jasiewicz et al., 2013; Jasiewicz and Stepinski, 2013).

Geomorphons have been shown to be useful for many mapping and modeling problems. For example, Libohova et al. (2016) demonstrated the value of the classification method for predicting soil properties on a glacial moraine while Sărășan et al. (2019) documented its use for drumlin extraction. Chea and Sharma (2019) noted association of geomorphons with socio-economic and built-environment characteristics.

2.2.6. Topographic aspect, insolation, and moisture

The orientation of topography with respect to incoming solar energy is an important control on geomorphology, hydrology, and landscape ecology (Gallardo-Cruz et al., 2009; Kumari et al., 2020; Langston et al., 2015; Pelletier et al., 2018). Table 2 lists and provides descriptions or equations for a selection of the most common variables associated with topographic aspect, solar insolation, or moisture while Fig. 4 shows some examples. Topographic aspect (Asp) represents the compass bearing or direction that a slope is facing (Chang, 2008; Hengl et al., 2009; MacMillan and Shary, 2009; Wilson and Gallant, 2000). Asp and associated measures are particularly useful for hydrologic and ecological modeling tasks, since aspect is related to the amount of solar insolation, sun exposure, subsurface moisture content, and, in some cases, precipitation at a site (Bennie et al., 2008; Ironside et al., 2018; Evans and Cushman, 2009; Franklin, 2020; Stage, 1976). For example, Evans and Cushman (2009) used a variety of aspect-related variables to aid in the prediction of conifer tree species occurrence. One complexity with using Asp in a predictive model is its circular nature (e.g., a slope aspect of 359° is closer in orientation to 2° than an orientation of 10° is to 2°). As a result, it is common to transform Asp to a linear variable for inclusion in predictive modeling tasks. Examples include northwardness (AspN) (Stage, 1976), eastwardness (AspE) (Stage, 1976), and the topographic radiation aspect index (TRASP) (Roberts and Cooper (1989); Evans, 2021, Evans, 2020; Evans and Cushman, 2009; Roberts and Cooper, 1989).

Table 2
Land-surface parameters that characterize slope orientation, solar insolation, and moisture.

Land-surface parameter	Abbreviation	Description/equation
Topographic Aspect	Asp	$270 - \frac{360}{2\pi} \times \arctan^2(\frac{\partial z}{\partial x}, \frac{\partial z}{\partial y})$
Northwardness	AspN	sin(Asp)
Easterwardness	AspE	cos(Asp)
Topographic Radiation Aspect Index	TRASP	$\frac{1 - cos\left(\left(\frac{\pi}{180}\right) \times (\text{Asp} - 30)\right)}{2}$
Heat Load Index	HLI	Index for annual direct incoming solar radiation based on latitude, slope, and aspect
Site Exposure Index	SEI	$\text{Slp} \times \cos(\pi \frac{\text{Asp} - 180}{180})$
Topographic Wetness Index	TWI	$\text{Ln}(\frac{Contriubting\ Area}{tan(Slp)})$

The heat load index (HLI) provides further refinement by incorporating latitude, Slp, and Asp to estimate potential annual direct incident radiation (McCune and Keon, 2002). The HLI calculation suggested by McCune and Keon (2002) transforms Asp so that the largest values are associated with southwest orientations, the warmer orientation in the northern hemisphere, and the lowest values are associated with northeast orientations, the cooler slopes. Similarly, the site exposure index (SEI) estimates solar insolation by rescaling Asp relative to a north-south axis and then multiplying by Slp (Ironside et al., 2018; Franklin, 2020).

The topographic wetness index (TWI) takes into account contributing area, which is discussed below, as a measure of surface or shallow subsurface flow accumulating at a cell location, and topographic slope, as a measure of how easily or quickly moisture leaves a cell. TWI has been shown to be useful when the phenomenon of interest is likely affected by moisture conditions, such as mapping vegetation communities and wetlands (Corcoran et al., 2011; Ironside et al., 2018; Evans and Cushman, 2009; Franklin, 2020; Moore et al., 1993).

For ecological mapping and modeling tasks, it is often desirable to incorporate variables that have clear associations with abiotic conditions that impact ecological processes and community composition (Ironside et al., 2018; Dyer, 2019). Examples of these are the water balance at a site—as estimated from temperature and radiation, which drive moisture demand, and precipitation and soil water storage, which dictate water availability (Dyer, 2019). Methods have been developed to estimate water balance-related measures; however, additional data beyond a DLSM are required. For example, Dyer (2019) developed an ArcGIS toolbox to generated raster-based estimates of monthly potential evapotranspiration, representing demand, based on the Thornthwaite approach (Mather, 1978) and the Turc equation (Turc, 1961). Input data requirements include DLSMs, soil available water capacity derived from digital soil datasets, temperature and precipitation estimates, such as those provided by PRISM (https://prism.oregonstate.edu/), global horizontal irradiance, and relative humidity. The DLSM data specifically are used to estimate monthly total radiation at each cell using the hemispherical viewshed algorithm (Rich et al., 1994; Fu and Rich, 2002). Once potential evapotranspiration is estimated, it is possible to generate estimates of actual evapotranspiration and water deficit or surplus monthly and annually (Dyer, 2019).

2.2.7. Surface hydrology

Calculating DLSM-based variables related to surface water hydrology is critical for analyzing and modeling the flow of water, sediment, and nutrients across landscapes (Böhner and Antonić, 2009; Chang, 2008; Gruber and Peckham, 2009). Fig. 5 illustrates variables associated with surface hydrology. In order to model the flow of water on the landscape

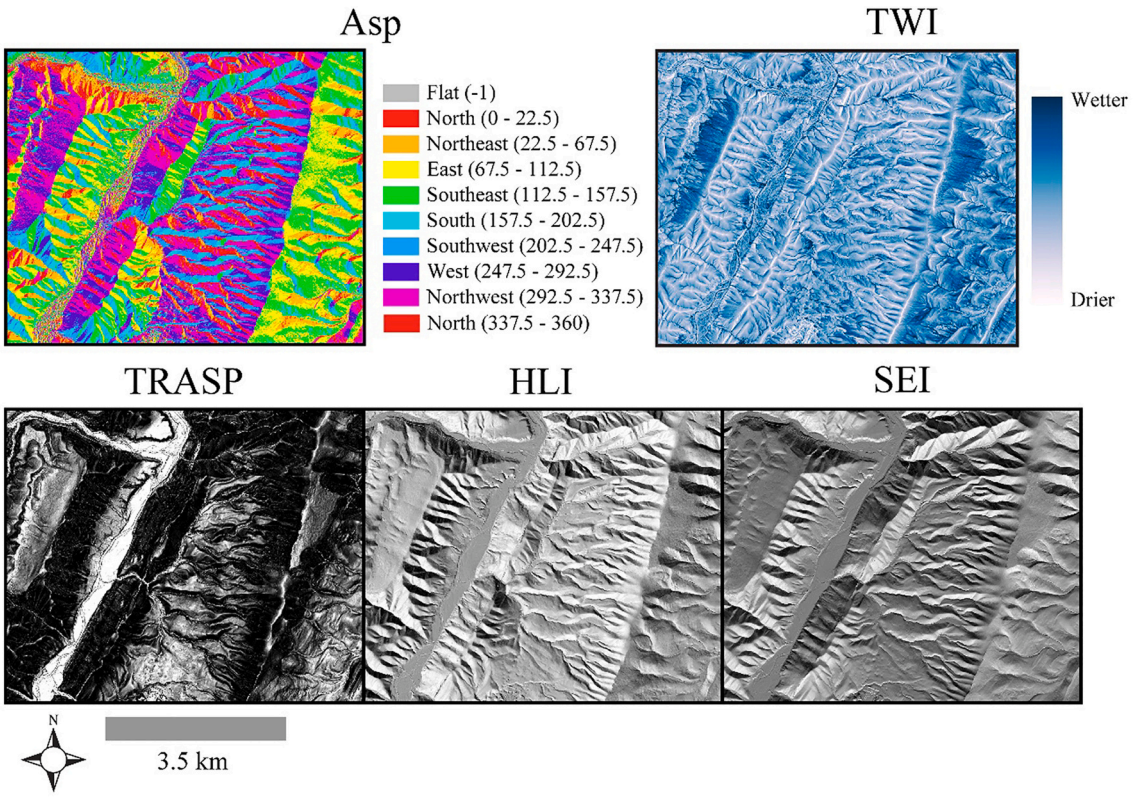

Fig. 4. Example metrics that characterize solar insolation and moisture. Asp = slope aspect, TWI = topographic wetness index, TRASP = topographic radiation aspect index, HLI = head load index, and SEI = site exposure index. Asp was calculated using ArcGIS Pro (ArcGIS Pro help—ArcGIS Pro | Documentation, 2021) while TRASP, HLI, and SEI were calculated using the spatialEco (Evans, 2020) package in R (R Core Team, 2020). TWI was calculated using SAGA (Olaya and Conrad, 2009).

surface and allow flow propagation through the entire drainage network, small depressions or pits can be removed to create a hydrologically corrected, or filled, DLSM. The depression filling process also allows identification of pits or sinks which may correlate with real topographic features of interest. Depressions in DTMs are often real rather than spurious and have important implications for hydrology and geomorphic processes (for example, in karst landscapes (Lyew-Ayee et al., 2007)). An alternative to pit filling that leaves depressions intact is to route flow through them using so-called "fill-and-spill" algorithms while leaving the DLSM itself unmodified (e.g., Barnes et al., 2021; Barnes et al., 2020; Callaghan and Wickert, 2019).

Flow direction (FlowDir) represents the direction of flow from a cell into one or multiple adjacent cells based on elevation differences between each cell and its neighbors. Flow accumulation (FlowAcc), or contributing area, counts the number of cells or amount of land area that contributes flow to each cell. Different algorithms are available to make these calculations; for example, the D8 method (single-flow-direction routing considering eight neighbors) only allows for flow to be directed to one adjacent cell while the D-Infinity method (a multiple-flow-direction method) allows for flow partitioning to multiple neighboring cells (Chang, 2008; Gruber and Peckham, 2009; Tarboton et al., 2016; Tarboton, 2005; Tarboton, 1997). Qin et al. (2007) proposed an augmentation of multiple-flow direction algorithms, which was subsequently implemented in ArcGIS Pro, that allows for adaption of the flow-partitioning exponent based on local land surface characteristics. Some issues have been documented with the D8 and other single-flow-direction methods including generation of parallel lines along principal directions; the inability to model divergent flow over convex slopes and ridges; and poor performance in highly variable topography, floodplains, and wetlands (Chang, 2008). Many of these issues have been addressed by various other flow routing schemes (see Wilson et al. (2007)). In general, D-Infinity is the most commonly used algorithm for applications in small drainage areas and/or in low-gradient areas where sheet or divergent flow may occur (Wilson et al., 2007).

Once FlowDir and FlowAcc raster grids are created, a variety of additional outputs can be derived from them. By setting a flow accumulation threshold or a slope-area threshold (Montgomery and Foufoula-Georgiou, 1993), a synthetic stream network can be generated. Next, each individual segment in the drainage network can be assigned a unique code, a product known as stream link (StrmL). Other products include stream order (StrmO), flow distance, or the upstream or downstream distance to a cell along the flow path, watershed or catchment boundaries (Chang, 2008; Gruber and Peckham, 2009; Tarboton et al., 2016; Tarboton, 2005, Tarboton, 1997), and indices of channel form—such as steepness—that might reveal geologic and geomorphic conditions (e.g., Kirby and Whipple, 2012; Perron and Royden, 2013).

It has been noted that traditional methods of generating surface hydrologic variables, such as FlowDir and FlowAcc, may be suboptimal for processing high spatial resolution and detailed digital terrain data, such as those derived from LiDAR. This results from the high level of local detail or noise as well as the difficulty in hydrologically correcting such surfaces. As a result, new methods are being developed and investigated to analyze such data (Clubb et al., 2014; Passalacqua et al., 2010; Pelletier, 2013). As one representative example, Sangireddy et al. (2016) introduced the open-source GeoNet software for generating surface hydrologic variables using a combination of nonlinear filtering, detecting channelized cells using a statistical analysis of surface curvature, and detecting channel heads and channel networks using a geodesic minimization principle.

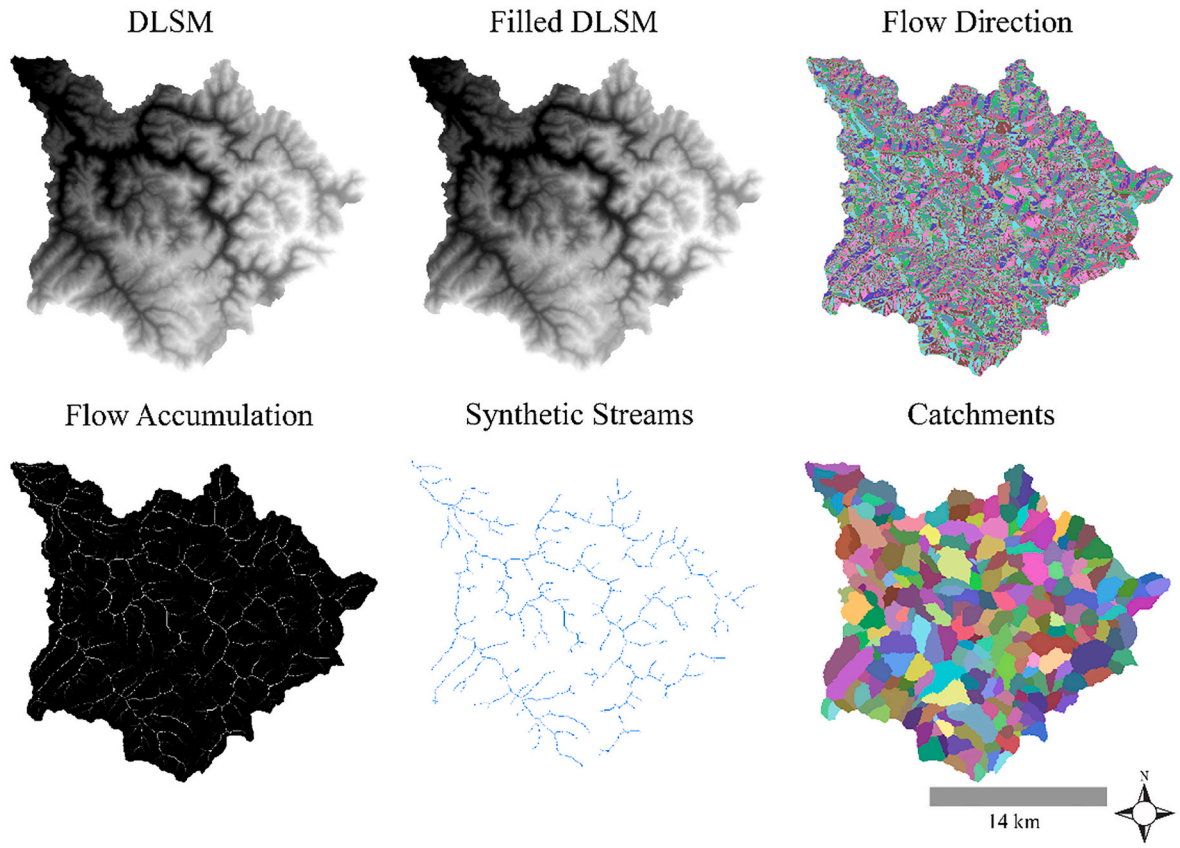

Fig. 5. Example surface hydrologic derivatives. All metrics were calculating using ArcGIS Pro (ArcGIS Pro help—ArcGIS Pro | Documentation, 2021). Results are for a catchment in West Virginia, USA.

3. Considerations for calculating, selecting, and implementing land-surface parameters for empirical modeling

3.1. Selecting variables

3.1.1. Selecting land-surface parameters overview

The large number of variables that can be derived from DLSMs to characterize the landscape surface complicates the process of selecting variables for inclusion in empirical predictive modeling or mapping tasks. Lecours et al. (2017) suggest that land-surface parameters are generally highly correlated and that a subset of six or seven carefully selected measures will capture most of the information content present in the DLSM data; however, this may not hold true for all mapping or modeling tasks, and the optimal feature subset may not be readily evident. Franklin (2020) and Xiong et al. (2021) suggests that land-surface parameter selection should be guided by what topographic factors influence the phenomenon being studied, modeled, or mapped, and Franklin (2020) further suggests additional guidance from existing literature, visual and statistical exploration of the DLSM data, and field observations. This section is structured with that framework in mind. Table 3 highlights some of the parameters discussed above with example uses and associations with landscape and geomorphic processes.

Existing literature can offer guidance; however, prior research often offers conflicting advice. For example, studies have consistently noted the value of Slp for mapping and predicting wetland occurrence (e.g., Maxwell et al., 2016; Wright and Gallant, 2007). In contrast, TWI, which would logically be considered for wetland prediction due to the likely association with areas of high flow accumulation, has been shown to be useful in some studies but not others. Rampi et al. (2014) and Knight et al. (2013) both note the value of TWI while Maxwell et al. (2016) and Wright and Gallant (2007) found the variable to be of little value. It is not always clear why certain variables are found to be useful or only useful in some studies; this could relate to differences in the presentation of features in different landscapes, the modeling methods or algorithms being used, and/or the characteristics of the DLSM data. For example, Maxwell et al. (2016) noted a high degree of local noise in TWI for their probabilistic wetland mapping in West Virginia, USA. This local noise may have reduced the value of the variable. Smoothing the TWI values or the original DLSM may have reduced local noise and increased the predictive value of the variable in the model (Maxwell et al., 2016).

Similarly, there does not appear to be a consensus as to the most useful variables for predicting slope failure, or landslide, susceptibility or occurrence. Generally, the incorporation of land-surface parameters has been shown to improve models; for example, Goetz et al. (2011) noted that empirical models that incorporate land-surface parameters as predictor variables often outperform methods that rely on physical models of slope failure. Slp, Asp, and surface curvatures have consistently been shown to have value for slope failure predictive modeling (Gessler et al., 1995; Goetz et al., 2015; Goetz et al., 2011; Maxwell et al., 2020c). However, a consistent, optimal set of variables that goes beyond this list has not been identified, and suitable predictors may depend on the landscape being predicted and/or the nature of the slope failures present. It may therefore prove useful to use feature selection methods to find the variables most effective for a particular study.

3.1.2. Variable selection methods and considerations

Reducing the size of the feature space offers a number of potential benefits, including minimizing the computation and memory requirements for training models, generating simpler or more parsimonious models for interpretability and reproducibility, and/or minimizing problems arising from the “curse of dimensionality” (James et al., 2013; Maxwell et al., 2018). The “curse of dimensionality”, or

Table 3
Land-surface parameters and example uses and associations with landscape characteristics and geomorphic processes. This table summarizes content presented in Section 2 and also draws from prior texts (e.g., Hengl and Reuter, 2009; Wilson and Gallant, 2000), reviews (e.g., Florinsky, 2017; Ironside et al., 2018; Franklin, 2020; Sofia, 2020; and Xiong et al., 2021), and Minár et al. (2020).

Group	Land-Surface Parameter	Example uses and associations
Steepness	Slope	Geohazards, sediment transport, erosion rates
Surface Curvature	Plan curvatures	Dispersion of materials and energy across the slope, cross-slope landforms
	Profile curvature	Movement of material and energy downslope, down-slope landforms, geohazards, geomorphic process dominance
	Twisting curvatures	Twisting of mass flow, geologic structures, underlying geology, process domain boundaries
Local Topographic Positions	Topographic position index	Ridge vs. valley, hillslope-scale processes, environmental gradients
	Topographic roughness index	Underlying geology, geomorphic process dominance, impact of surface processes over time
Rugosity	Surface relief ratio	State of relief, location of tectonic and lithologic boundaries, state of topographic transience
	Surface area ratio	Slope breaks, rock outcrops, scarps
Incision	Topographic dissection index	Recent stream incision, fluvial processes and erosion, state of topographic transience
Orientation	Aspect	Incoming solar radiation, sun exposure, subsurface moisture content, precipitation
	Northwardness	Same as Asp, but a linear variable
	Eastwardness	Same as Asp, but a linear variable
Insolation	Topographic radiation aspect index	Incoming solar insolation and moisture content
	Heat load index	Potential annual direct incident radiation, energy availability, vegetation communities
	Site exposure index	Incoming solar radiation based on aspect and slope, energy availability, vegetation communities
Moisture	Topographic wetness index	Steady state moisture, mapping of vegetation communities and wetlands
	Flow accumulation	Amount of flow accumulating to a location, moisture content, stream initiation, river discharge, process transition from hillslope to fluvial dynamics

Hughes phenomenon, is the observation that increasing the number of predictor variables beyond a threshold sometimes decreases the accuracy of models because, even though more information is potentially provided, the problem must be solved in a larger, more complex feature space. This issue is of particular concern when a small number of training samples is available to characterize a complex feature space (i.e., a dataset with many variables) (Hughes, 1968). Some methods are particularly susceptible to this problem; for example, *k*-nearest neighbor (*k*-NN) classification accuracy generally declines as the feature space becomes very large, while random forest has generally been shown to be more robust (Maxwell et al., 2018).

Given the complexity of this topic, a complete treatment of feature selection methods is outside the scope of this review. For reviews focusing on feature selection methods, please see Chandrashekar and Sahin (2014), Khalid et al. (2014), and Cai et al. (2018). We provide a brief review here. Supervised feature selection methods, which rely on labeled data, can be grouped into three broad categories: filter, wrapper, and embedded methods. Filter methods use a statistical measure to rank variables and assess the correlation between each predictor variable and the response variable. Examples include correlation coefficients and the mutual information metric. Advantages of filter methods are that they can be computationally light and avoid overfitting to the training data; however, not all measures take into account correlation between predictor variables, which can result in redundant computations or a suboptimal feature space. Also, the learning algorithm is not considered, so the selected feature space may not be optimal for a specific learning algorithm (Guyon and Elisseeff, 2003; Chandrashekar and Sahin, 2014; Khalid et al., 2014; Cai et al., 2018). In contrast to filter methods, wrapper methods use the learning algorithm and resulting model performance, as measured with assessment metrics, to select features. This requires testing different predictor variable combinations, which can be computationally intensive, slow, or unfeasible. In order to alleviate the need to test all variable combinations, heuristic methods have been proposed, such as genetic algorithms (Goldberg, 2006) and particle swarm optimization (Kennedy and Eberhart, 1995), which may not yield the optimal variable subset but offer an approximation that can be feasibly calculated. In order to suggest a single subset, different methods are available to add or remove variables. For example, backward selection iteratively removes variables from the full set while forward selection iteratively adds variables. Issues with wrapper methods include computational intensity, which is only partially alleviated using heuristic methods, and the possibility of overfitting to the training data, or reduced generalization to new samples (Chandrashekar and Sahin, 2014; Khalid et al., 2014; Cai et al., 2018). Lastly, embedded methods incorporate the feature selection process as a component of model training (e.g., recursive feature elimination methods using SVM or RF). There are also unsupervised or semi-supervised methods, which can be used when a full set of labelled training data are not available (Law et al., 2004; Chandrashekar and Sahin, 2014; Khalid et al., 2014; Cai et al., 2018).

Other than the considerations outlined above, there are some other key factors to consider when choosing a feature selection method including the impact of variable correlation and the stability of the result. Stability relates to the consistency in selected features when using different training datasets or subsets. Kalousis et al. (2005) and Chandrashekar and Sahin (2014) both offer discussions of stability while Dunne et al. (2002) suggest solutions to this issue for wrapper methods specifically. It is also sometimes of interest to take into account not just model performance but the complexity of the model. A model using less predictor variables may be desirable due to reduced computational time and model complexity at the expense of a slight reduction in accuracy. For example, Murphy et al. (2010) integrated a parameter into a random forest-based variable select process that allows the user to specify the level of reduced accuracy that is acceptable in order to increase parsimony. This method is available in the R (R Core Team, 2020) rfUtilities package (Evans and Murphy, 2015). Georganos et al. (2018) documented that the feature selection method used can impact both model accuracy and parsimony. They proposed a metric, classification optimization score (COS), that takes into account both model accuracy and parsimony with the goal of selecting a feature space with minimal processing time and storage while maintaining accuracy.

A key issue associated with selecting a subset of variables is determining the importance of variables for the task of interest. As noted by Debeer and Strobl (2020) the concept of variable importance in machine learning and predictive modeling is not generally clearly defined. Marginal importance is the impact of a specific predictor variable on the dependent variable without considering the other variables in the model. In contrast, partial or conditional importance is the added value gained by including a specific predictor variable for predicting the dependent variable considering all other variables in the model. When no correlation exists between the predictor variables, marginal and partial importance are equivalent (Debeer and Strobl, 2020).

As an example, within the RF framework variable importance can be assessed by randomly permutating the values associated with a specific

variable then predicting the withheld, or out-of-bag, data. With this random permutation of the variable, greater decreases in model performance for predicting the withheld data, or increases in the misclassification rate, serve as an estimate of variable importance (Breiman, 2001). When variables are correlated, this measure cannot be interpreted as a truly marginal or partial importance estimate (Strobl et al., 2007; Strobl et al., 2008; Debeer and Strobl, 2020). Although it cannot be interpreted as one of these endmembers, Strobl et al. (2008) suggest that it is a more marginal estimate of importance. Strobl et al. (2008, 2009), with additional augmentations presented in Debeer and Strobl (2020), introduce a variable importance estimation method based on a conditional inference trees implementation of RF and the permutation-based importance estimation process that provides estimates of both partial and marginal importance. However, these importance estimates remain an approximation, as obtaining true marginal or partial importance is difficult due to the complexity of the DT ensemble and the difficulty of completely accounting for predictor variable correlation (Strobl et al., 2008; Debeer and Strobl, 2020). This method is implemented in the R (R Core Team, 2020) party (Strobl et al., 2009) and permimp (Debeer and Strobl, 2020) packages.

3.1.3. *Variable reduction methods*

As an alternative to selecting a subset of important variables from the feature space, it is also possible to generate new features from the original predictor variables. This process is generally termed feature reduction. Example methods include independent component analysis (ICA) (Hyvärinen and Oja, 2000), isomap embedding (Silva and Tenenbaum, 2002), and spatial sign processing (Serneels et al., 2006). The recipes package (Kuhn and Wickham, 2021), which is part of tidymodels (Kuhn and Wickham, 2020) in R (R Core Team, 2020), offers implementations of a variety of feature reduction methods for use in machine learning research and processing pipelines. One common feature reduction method is principal component analysis (PCA), in which the goal is to transform the original variables into new, uncorrelated features defined by linear combinations of the input features. The underlying assumption is that correlated variability is a measure of the importance of information, and that this can be used to identify a subset of the transformed, decorrelated variables that summarizes the majority of the original variance (F.R.S, 1901).

As an example of the use of PCA, Fig. 6 shows a correlation matrix for a subset of 12 land-surface parameters calculated within our example study area near Seneca Rocks in West Virginia, USA. Correlations were calculated using Spearman's rank correlation (Zar, 1972). The figure shows that the variables are generally not strongly correlated with each other (they are mostly represented by colors close to white), though Slp is strongly positively correlated with TRI and SAR, and ProCrv and TDI both tend to be correlated with TPI and SRR, as indicated by blue colors. In contrast, TRI, SAR, and Slp are all strongly negatively correlated with TRASP, as indicated by red colors. Despite the impression from Fig. 6 that most variables are not strongly correlated, the scree plot (Fig. 7) demonstrates that a large proportion of the variance in the dataset is explained by a subset of principal components. The first principal component explains 25.9% of the total variance in the data while the first seven collectively explain 91.6% of the variance. This suggests that the 12 variables have considerable redundancy.

3.1.4. *Explaining models and feature contribution*

A critique of machine learning methods – such as RF, SVM, and ANN – is their black box nature (James et al., 2013; Maxwell et al., 2018). Although ancillary output, such as variable importance estimates, can increase the interpretability of models, there has been a recent push for more interpretable machine learning. Nori et al. (2019) suggest a framework to make black box predictions more interpretable and suggest the use of (1) the LIME method, which attempts to explain individual predictions using a linear and local approximation of a model and allows for interpreting feature contributions additively, and (2) SHAP

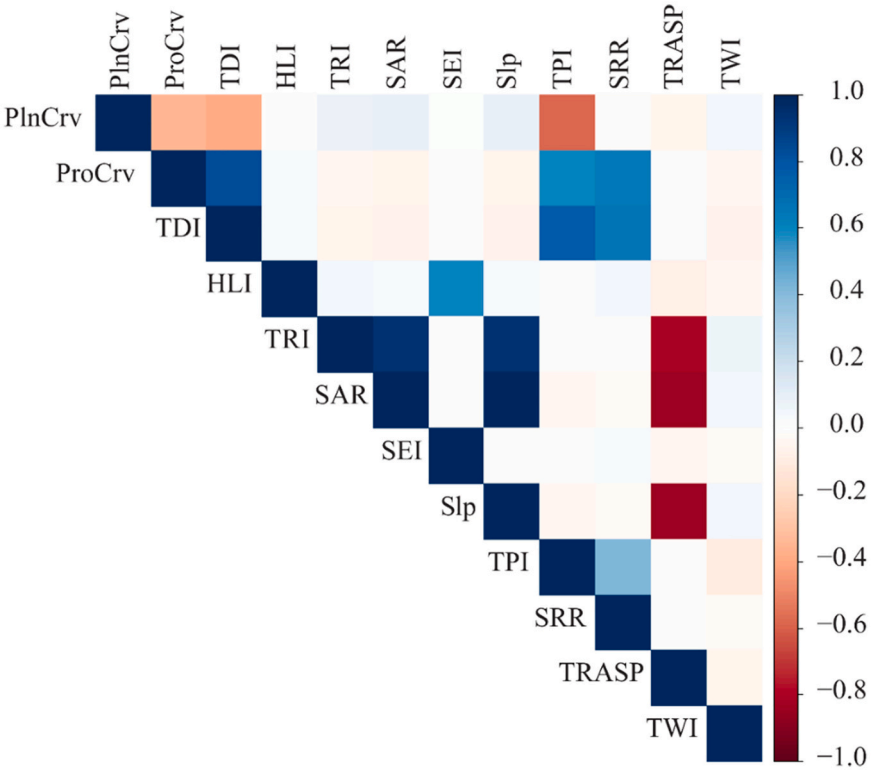

Fig. 6. Correlation matrix for a set of 12 land-surface parameters derived from a DLSM. Darker red indicates a stronger negative correlation while darker blue indicates stronger positive correlation. Correlation was calculated using Spearman's rank correlation. (For interpretation of the references to colour in this figure legend, the reader is referred to the web version of this article.)

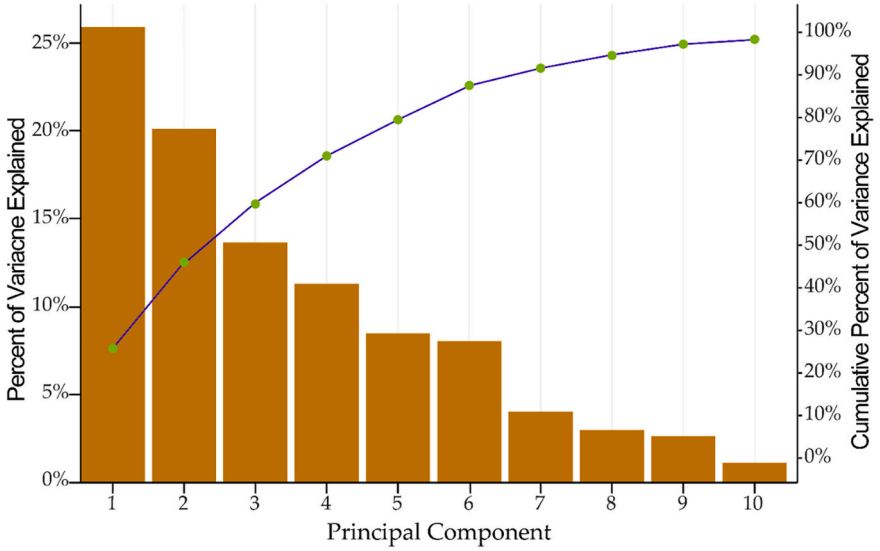

Fig. 7. Scree plot describing the percent of variance in the original variables explained by the first ten principal components.

(Shapley Additive Explanations) values, which offer a measure of variable importance using cooperative game theory. They also suggest using sensitivity analysis and partial dependency plots to further explain models (Lundberg et al., 2019; Lundberg and Lee, 2017; Nori et al., 2019). Partial dependency plots visualize how the dependent variable is impacted by a single predictor variable. To accomplish this, the dependent variable is predicted using a model in which values for the predictor of interest are maintained while the other variables are replaced with their average value (Friedman, 2001).

Recently, the explainable boosting machine (EBM) algorithm has been proposed as a fully interpretable, or glass box, predictive model. EBM is a generalized additive model (GAM) where the function associated with each feature is estimated using bagging or gradient boosting and training on one predictor variable at a time using a low learning rate. The contribution of each predictor variable in the model can be explored by plotting the resulting function to show how values of the predictor variable correlate with the predicted outcome value (Nori et al., 2019).

Fig. 8 shows some example outputs generated alongside the EBM model for a prediction of slope failure occurrence based on LiDAR-

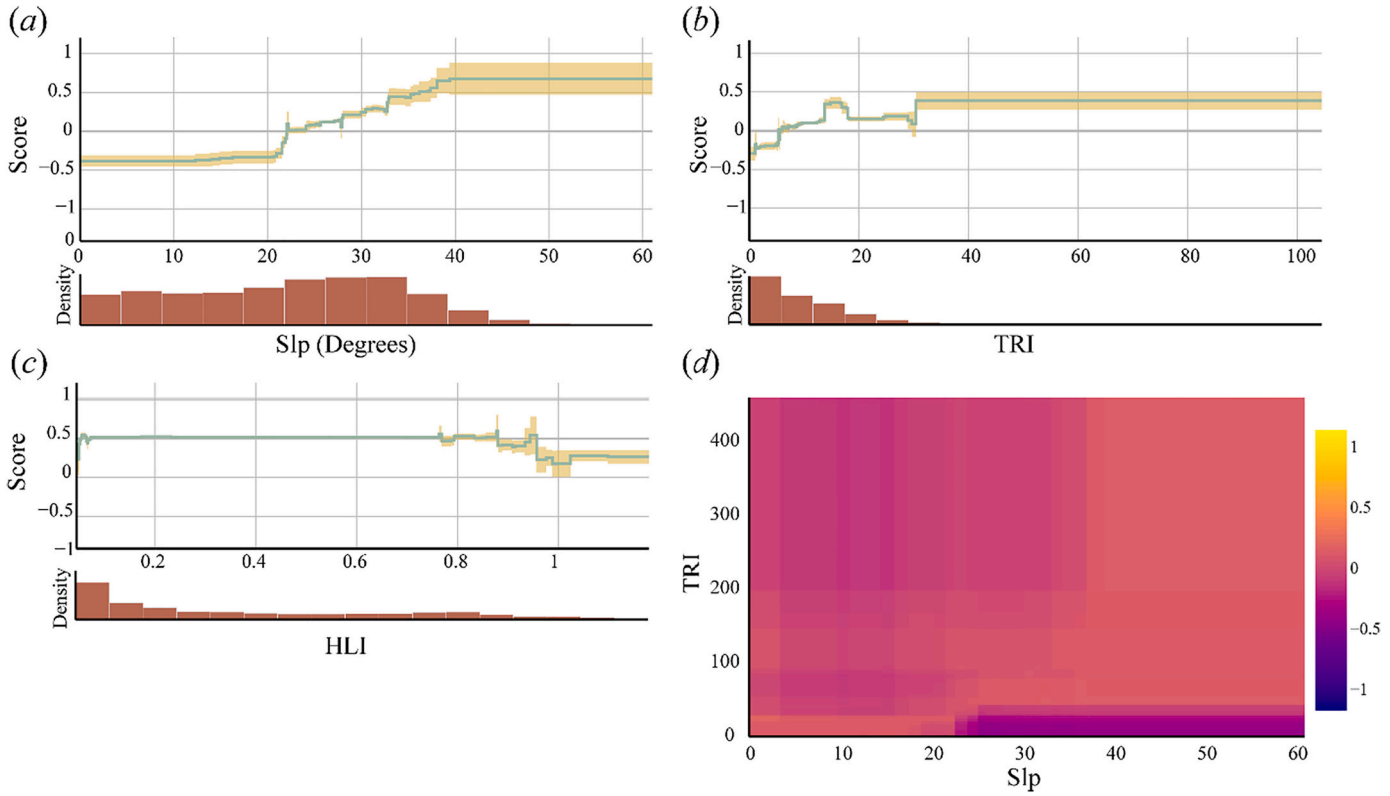

Fig. 8. Example plots associated with explainable boosting machines (EBM). A score of 1 indicates a predicted high likelihood of slope failure occurrence while −1 indicates a high likelihood of not slope failure occurrence. (*a*) Slope (Slp) impact on resulting prediction. (*b*) Topographic roughness index (TRI) impact on resulting prediction. (*c*) Heat load index (HLI) impact on resulting prediction. (*d*) Interaction between Slp and TRI.

derived land-surface parameters. These data are from a probabilistic prediction of slope failure occurrence for the Valley and Ridge region of West Virginia (Maxwell et al., 2020c). Steeper slopes (Fig. 6(*a*)) and greater topographic roughness values (Fig. 6(*b*)) are associated with slope failures. A score of 1 suggests a high predicted probability of slope failure occurrence. HLI is not very predictive of slope failure occurrence (Fig. 6(*c*)) since there is little variability in the slope failure prediction with changes in this variable. The EBM model can also incorporate interactions; for example, Fig. 6(*d*) describes the interaction between Slp and TRI for predicting slope failures. Steeper slopes tend to be less associated with slope failure occurrence if rugosity is low.

3.2. Spatial resolution, level of detail, and moving windows

3.2.1. DLSM spatial resolution and level of detail

As more digital elevation datasets become available, more choices exist for input data for analyses. Factors to consider in choosing data include spatial resolution (i.e., the cell size of the input DLSM) and the associated level of detail (i.e., the smallest landscape units or features that can be discerned, which is impacted by the spatial resolution and amount of smoothing or generalization resulting from data collection and pre-processing operations), as well as geographic coverage and consistency. High spatial resolution, LiDAR-derived data are not yet globally available, whereas some moderate resolution datasets, such as ASTER GDEM, provide near-global coverage, which is important to ensure consistent mapping or modeling in projects that cover large extents. LiDAR data collected with different sensors, collection parameters, or flight specifications will have different levels of detail. If raster-based DLSMs are generated from datasets such as LiDAR-derived point clouds, the analyst must choose an interpolation method (e.g., inverse distance weighting (IDW), spline, or kriging) and the output spatial resolution or cell size. It might also be desirable to resample, aggregate, or generalize high spatial resolution data. For example, data may be generalized using a mean or Gaussian moving window filter (Chang, 2008; Lillesand et al., 2015; Pike et al., 2009; Reuter et al., 2009; Wilson and Gallant, 2000). Some recent studies have argued for using TINs to calculate land-surface parameters given their multi-scale nature (Hu et al., 2021a, 2021b). Customarily, TINs have been converted to raster-based DLSMs prior to the calculation of parameters; however, Hu et al. (2021a, 2021b) argue that methods should make use of the vertices defining the TIN facets. Future work in this area may aid in improving the characterization of land surfaces at variable scales.

The level of detail, spatial resolution, and cell size of a dataset may or may not impact resulting model performance. For example, Knight et al. (2013) found that the source and spatial resolution of DLSM data had little impact on wetland mapping results and that the inclusion of terrain derivatives —regardless of their spatial resolution and source — improved classification performance over just using optical data. Similarly, Maxwell and Warner (2019a, 2019b) compared DLSMs from different sources (LiDAR vs. photogrammetry) and spatial resolutions (1 m, 3 m, and 10 m) as input for probabilistic prediction of wetland occurrence and found that neither the source nor the spatial resolution had a large impact on the resulting model accuracy, though finer spatial resolution data were generally more useful for mapping smaller wetlands. In contrast to these studies, Brock et al. (2020) suggest that the source and spatial resolution of digital elevation data impact the accuracy of landslide susceptibility models and call for greater care in selecting input DLSM data for such tasks. We argue that the importance of source and spatial resolution will partially depend on the landscape features or patterns being monitored. For wetland mapping, general characteristics, such as Slp and topographic position, may be predictive of occurrence and be adequately characterized with coarser and/or more generalized data. In contrast, landslide susceptibility models may require more detailed datasets to characterize predictive patterns, such as scarps, slope breaks, and geologic unit contacts.

Regardless of whether or not the final output model, prediction, or map is affected by the source and spatial resolution of the digital elevation data, these properties do affect land-surface parameter values (Habib et al., 2018; Kienzle, 2004; Sărășan et al., 2019). Habib et al. (2018) documented impacts of DLSM spatial resolution, interpolation, and filtering on the accuracy of the estimated elevation surface. Moore et al. (1993) and Kienzle (2004) both document impacts of spatial resolution on a variety of calculated derivatives, including Slp, Asp, PlnCrv, ProCrv, and TWI. Kienzle (2004) conclude that the optimal raster cell size depends on the complexity of the land surface and the parameters calculated. Sărășan et al. (2019) noted the impact of spatial resolution on calculating geomorphons to support the mapping of drumlins.

3.2.2. Moving windows and land surface characterization at multiple scales

Several decisions must be made when defining a moving window or kernel over which to calculate land-surface parameters (Fig. 9), leading to an effectively infinite number of possible parameter combinations. Possible window shapes include circles, rectangles or squares, and annuli. The size of the window is specified differently depending on the shape used. Circular window size is defined using the radius while rectangular or square window size is defined using the height and width. An annulus window size is defined using an inner and outer radius. Units are generally length units, such as meters, or number of cells. Once a shape and size are selected, it is generally possible to apply different weighting techniques to control the relative impact of each cell within the window on the resulting calculations. Using no weighting implies that all cells will have the same weight no matter their distance from the center cell, while the weights in a linear model decline linearly with distance from the center cell. In inverse distance weighting (IDW) the weighting is inversely proportional to the distance to the center cell raised to a specified power. Higher powers put more weight on cells nearer to the center cell (Chang, 2008). Other options include exponential and Gaussian weighting (Chang, 2008; Lillesand et al., 2015).

Weighting methods are not available in all software tools. One notable exception is SAGA; for example, the TPI calculation available in this tool allows a selection from no weighting, IDW with variable powers, exponential, or Gaussian (Olaya and Conrad, 2009). Also, the Landserf software offers tools for selecting window sizes and assessing sensitivity (Wood, 2009). Recently, the ArcGIS Pro software has added the Surface Parameters Tool, which can be used as a replacement for the Slope, Aspect, and Curvature tools. In contrast to these tools, Surface Parameters allows for changing the square window size and is not limited to a 3-by-3 m window. Further, it can make use of an adaptive neighborhood in which the window size used at each cell location can vary based on the local variability in elevation. At locations with more local variability, a smaller window size will be used whereas a larger window size will be used when local variability is lower. A user can define the largest allowed window size, and the tool will adjust the window size for each moving window in an attempt to minimize surface variability while maintaining the largest window size possible (ArcGIS Pro help—ArcGIS Pro | Documentation, 2021; Wilson and Gallant, 2000).

Fig. 10 compares TPI calculations using different window shapes (circle, square, and annulus) and sizes with no weighting or adaptive neighborhood applied. Similar landscape patterns are represented irrespective of the parameters used; for example, higher values indicate more prominent topographic positions, such as ridges, and lower values indicate lower positions, such as valleys. Visually, the shape of the window has less impact than the size of the window, as increasing the cell size yields a more general representation that is less affected by local features.

Our review of published studies indicates that different window sizes and/or shapes are not commonly explored, and that many authors do not justify the window size and/or shape used, and in some cases do not even specify the size and shape used. On the other hand, some studies have used multiple window sizes in an attempt to characterize the land surface at multiple scales. For example, Maxwell et al. (2016), Maxwell

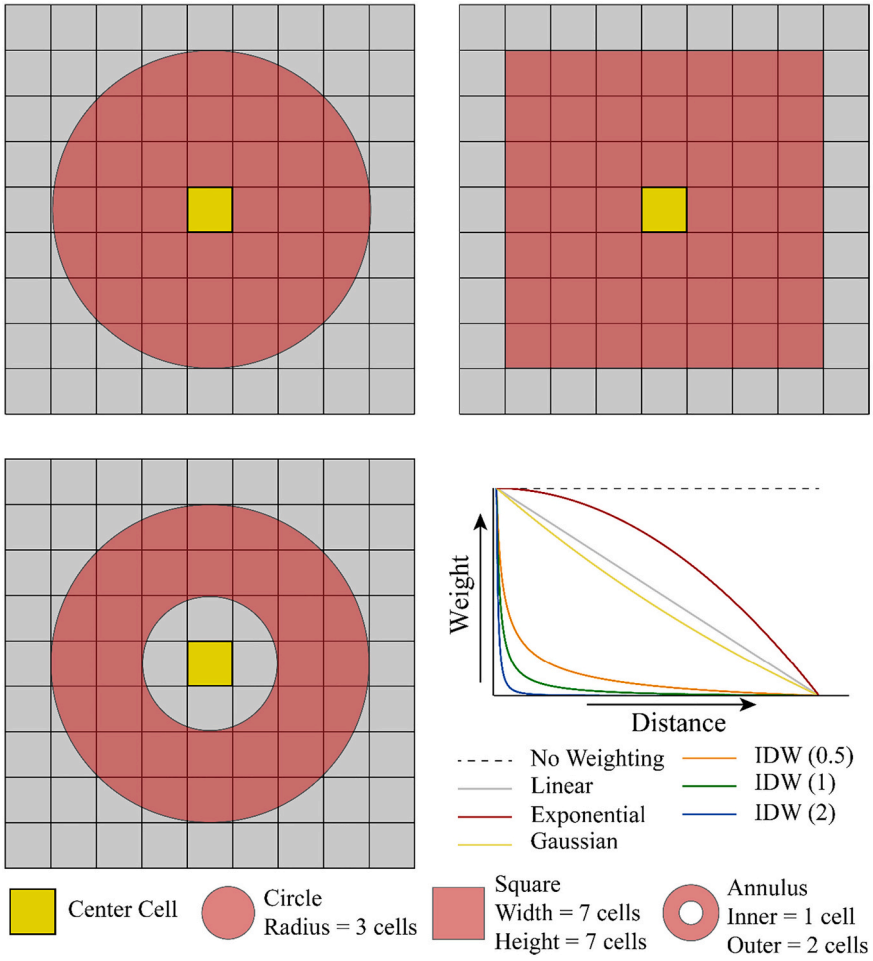

Fig. 9. Example window shapes and distance weighting methods.

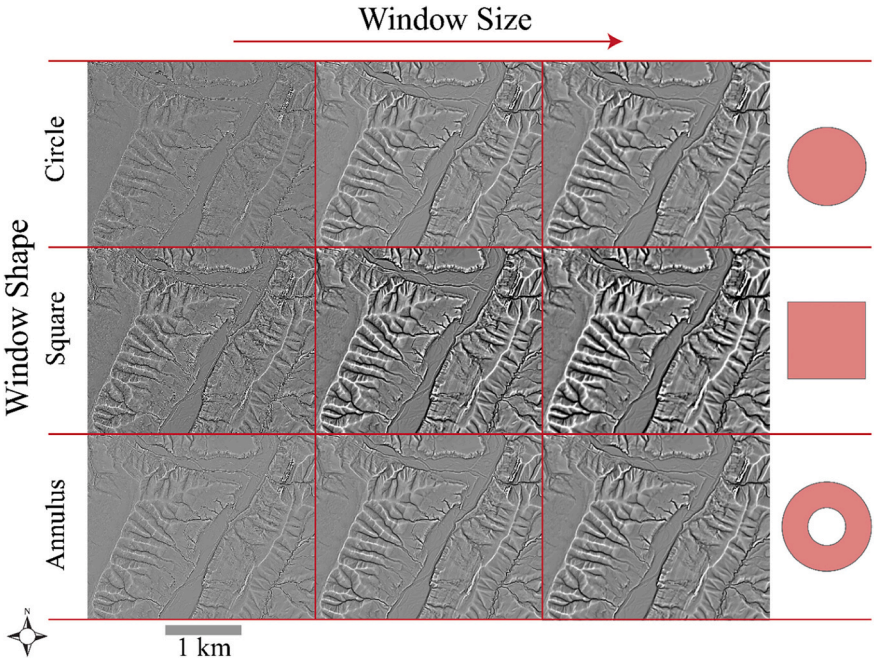

Fig. 10. Comparison of TPI calculated using different window shapes and sizes. TPI was calculated with circular radii of 7, 21, and 35 cells, square widths/heights of 10, 20, and 30 cells, and annulus windows with a 2-cell inner radius and 10-, 20-, and 30-cell outer radii.

and Warner (2019a, 2019b), Maxwell et al. (2020c), and Maxwell et al. (2021) used multiple window sizes, which were selected based on a consideration of typical ridge-to-valley distances within the landscape being studied. These studies justify this method based on the scale of interest, as they all were interested in summarizing patterns at the range of scales associated with typical hillslopes and were less concerned with local patterns or variability. Maxwell et al. (2016) and Maxwell and Warner (2019a, 2019b) also averaged the variables calculated across window sizes to generate a single summary metric. For the prediction of slope failure occurrence using digital elevation data and RF machine learning, Maxwell et al. (2020c) calculated a variety of metrics using circular windows, no weighting, and radii of 7, 11, and 21 cells from DLSM data with a 2 m spatial resolution. For this specific predictive modeling task, their results suggest that incorporating multiple scales generally improved model performance based on area under the receiver operating characteristic (ROC) curve; overall accuracy; and precision, recall, and F1 score for the slope failure class. Models trained using smaller window sizes (i.e., 7 or 11 cell radii) generally outperformed models using the larger 21 cell radius window size, highlighting the value of characterizing more local patterns for this specific task.

Albani et al. (2004) notes that the size of the window impacts both the resulting measures and the propagation of errors in the original DLSM-based elevation measurements through the modeling process. Measurements calculated using smaller window sizes tend to be more affected by elevation measurement errors. Further, errors or patterns resulting from the interpolation method used or patterns in the point or contour data used to generate the raster surface are more evident when using smaller windows. They suggest that the choice of window size is partially dictated by the tradeoff between minimizing the impact of error and obtaining the level of topographic detail desired. They also propose a method for assessing the loss of topographic detail based on an analysis of residuals and spatial autocorrelation in local windows.

Several methods have been investigated to determine optimal window sizes or to characterize the land surface at different scales or levels of generalization including changing the size of the moving window, using low-pass filters to generalize DLSMs, and reducing the spatial resolution via resampling. For the mapping of soil properties using land-surface parameters, it has been demonstrated that using appropriate scales or window sizes can improve predictive performance (Behrens et al., 2010; Behrens et al., 2018; Dornik et al., 2022). Behrens et al. (2018) propose a method of multi-scale landscape characterization, termed mixed scaling, that makes use of down-sampling the DLSM using Gaussian pyramid scaling, which relies on convolving a matrix of elevation values using a Gaussian blur filter. Rows and columns are then removed to generate octaves that represent the land surface at different scales. In order to transform the results back to the original spatial resolution, up-sampling is then performed by inserting rows and columns with zero values, reapplying a Gaussian filter, and multiplying by 4 to correct for the insertion of zero values. Additional intermediate scales can be generated using resampled versions of the original DLSM (Behrens et al., 2018). Behrens et al. (2018) and Dornik et al. (2022) argue that this method yields intuitive land-surface parameters without processing artifacts.

Drăguţ and Blaschke (2006), Drăguţ et al. (2011) and Drăguţ and Eisank (2011) explored geomorphic and landform mapping using geographic object-based image analysis (GEOBIA) methods in which terrain data are segmented into objects or regions of similarity and then later classified. Such methods require the analyst to consider the scale or scales of interest. Towards this goal, Drăguţ et al. (2011) proposed a scale selection method based on local spatial autocorrelation and local variance. The process involves up-sampling the gridded data using resampling or changing the scale parameter in the segmentation algorithm, calculating local variance within 3-by-3 cell windows or derived image segments, calculating a rate of change in local variance from one level to the next, and plotting the resulting values against the scale level. Peaks in this graph indicates scales that may have geomorphic meaning.

Other moving-window-like filtering operations that operate at a defined scale, such as wavelet transforms of the elevation field, can be used to identify geomorphic process dynamics from digital elevation models by extracting the dominant landforms at a variety of scales. These procedures are typically used to distinguish local-scale (e.g., motion along a single fault) from regional-scale (e.g., rock uplift driven by mantle dynamics) controls on topography (Moodie et al., 2018; Struble and Roering, 2021; Wegmann et al., 2007). Filtering the land surface with wavelet transforms removes the signature of all topographic features with a spatial dimension less than the chosen wavelength (e.g., Wegmann et al., 2007). Rather than choose a single wavelength *a priori*, most studies that filter topography to deduce geomorphic dynamics produce filtered DLSMs for a variety of filter wavelengths and compare the results to determine which landscape features persist as wavelength increases (e.g., Struble and Roering, 2021). These filtered DLSMs can then be interpreted by analysts or used as independent variables for predictive modeling.

3.3. Multi-temporal terrain data

The advent of widely available airborne and drone-based LiDAR data, as well as drone-based structure-from-motion photogrammetry, has led to a proliferation of studies that leverage multitemporal DSMs and DLSMs to assess landscape change—either natural (e.g., Cavalli et al., 2017; Croke et al., 2013; James et al., 2012; Perignon et al., 2013; Turowski and Cook, 2017; Yang et al., 2021) or human-induced (e.g., Maxwell and Strager, 2013; Ross et al., 2016)—over time. Fig. 11 provides an example of DLSMs of difference where two surfaces representing different terrain conditions from different dates are subtracted to quantify elevation gains and losses. This specific example relates to mountaintop removal surface coal mining in southern West Virginia, USA, which results in the excavation of mountaintops and the filling of adjacent valleys with displaced overburden rock material (Maxwell and Strager, 2013; Ross et al., 2016). The DLSM data pre- and post-mining were derived from LiDAR and are represented using HSs. The DLSMs were differenced to produce a DLSM of difference. A change threshold was then applied to differentiate areas of no change, elevation gain (fill), and elevation loss (cut or excavation). From such surfaces, it is possible to estimate land area and volumetric landscape change (Williams, 2012).

The magnitude of elevation change that can be detected by differencing DLSMs depends on the accuracy of the input DLSM data where the minimal level of detection is estimated from the root mean square errors (RMSEs) of the elevation measurements from the input DLSMs (Eq. (7)). Changes greater than the error threshold are deemed to have resulted from landscape change while differences below the threshold are assumed to be the result of error or noise. This method generally results in a conservative estimate of change. Another option is to use a confidence interval or probabilistic threshold calculated using the elevation differences and the combined error (Eq. (8)). Assuming a normal distribution allows for the calculation of t-values for a two-tailed Student's t-distribution and the determination of an appropriate elevation threshold to represent a desired confidence interval (e.g., 95%). It may be possible to detect changes below the error threshold if alterations are more widespread and larger than a single cell (Williams, 2012).

$$\text{Minimal Level of Detection} = \sqrt{(RMSE_{pre})^2 + (RMSE_{post})^2} \tag{7}$$

$$t = \frac{|z_{post} - z_{pre}|}{\sqrt{(RMSE_{pre})^2 + (RMSE_{post})^2}} \tag{8}$$

The amount of error may not be consistent across entire DLSM extents due to changes in the density of measurements, combination of

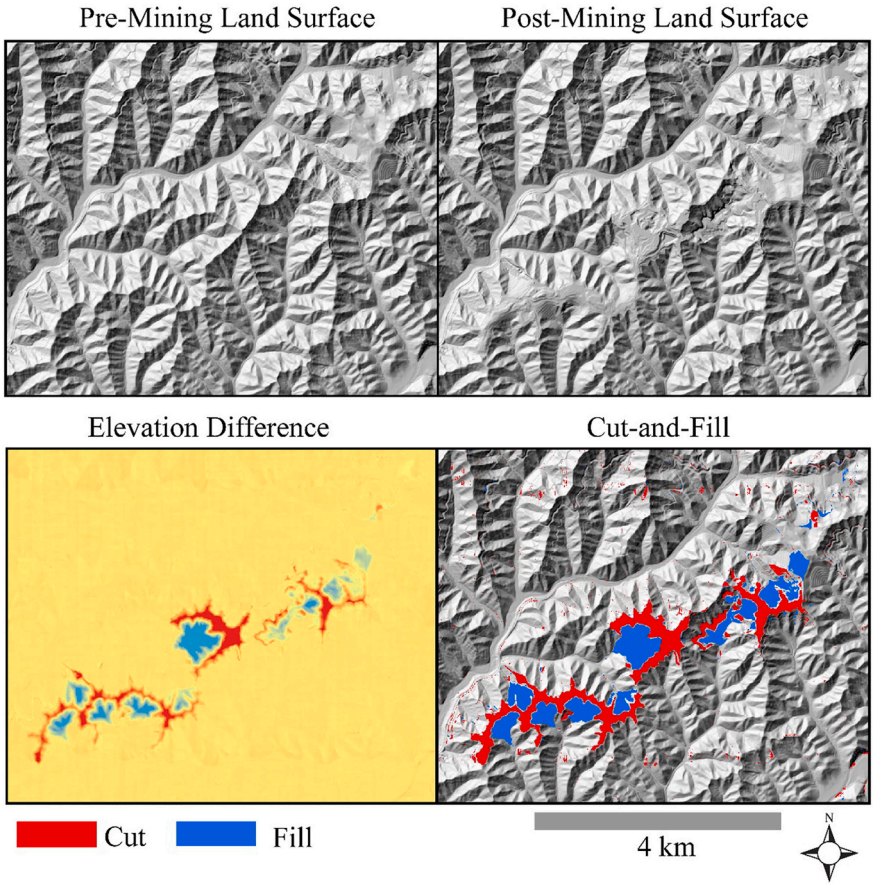

Fig. 11. Example multi-temporal DLSM analysis to assess topographic change resulting from surface coal mining in southern West Virginia, USA. The pre- and post-mining land surfaces were derived from LiDAR point clouds provided by the West Virginia GIS Technical Center (WVGISTC).

multiple data sources into a single DLSM, or changes in land cover or terrain conditions. For example, ground measurements under a tree canopy will likely be sparser in comparison to those in open areas for data interpolated from LiDAR point clouds. Estimates of subcanopy ground elevations are of specific concern when using methods that are not canopy penetrating, such as InSAR. More error is anticipated when comparing older, photogrammetrically-derived datasets with each other or with newer LiDAR-derived DLSMs. Uncertainty can also be caused by misregistration errors or co-registration errors between the datasets (Cavalli et al., 2017; Chang, 2008; Höfle and Rutzinger, 2011; James et al., 2012; Lillesand et al., 2015; Williams, 2012).

4. Recommendations and research needs

4.1. Recommendations

4.1.1. Feature selection and reduction

Predictive mapping and modeling require selecting predictor variables from among a bewildering array of DLSMs and DLSM-derived land-surface parameters. Variable selection can be guided by prior understanding of what landscape characteristics may impact the phenomenon being studied, modeled, or mapped with additional guidance from existing literature. If it is unclear what variables should be included, the recommended best practice is to undertake a pilot study over a manageable spatial extent or multiple extents that are representative of the landscape being investigated. As highlighted above, a variety of feature selection or reduction methods are available; however, it is important to consider strengths and weaknesses (e.g., computational time, impact of multicollinearity, overfitting, and consideration of parsimony) for specific tasks. When assessing variable importance, researchers and analysts must determine whether marginal importance, partial importance, or some mix of these end members should be assessed. For greater control over the assessment of variable importance, especially when predictor variables are correlated, we recommend the RF-based method proposed by Debeer and Strobl (2020) be considered. Recent advancements in explainable machine learning, such as EBMs (Nori et al., 2019), can also be used to better understand the response of the dependent variable to each predictor variable and each predictor's contribution to the resulting prediction.

One issue with undertaking a pilot study, performing feature selection, and/or performing feature reduction (e.g., generating uncorrelated variables with PCA) is that a large number of variables will need to be calculated to perform the analysis. The pilot investigation may speed up the later processes of optimizing models, training models, and inferring to new data over large spatial extents. However, the pilot study can still be complex and computationally intensive since a large number of land-surface parameters, including potentially repeated calculation of the same parameters at different scales, must be generated. In this case, a user may decide that an optimal feature space is not necessary if the set of variables included provides adequate performance based on assessment metrics and output. Or, analysts may be willing to accept a feature space that has not been optimized or evaluated if adequate results can be obtained without a pilot study or exploratory analysis.

4.1.2. Selecting and documenting input DLSM data

Selection of input DLSM data should be guided by the availability of consistent data covering the full extent of interest, the size or scale of the features or phenomenon being investigated, the level of detail or degree of generalization desired, and the accuracy and quality of the available data. Detailed, high spatial resolution surfaces, such as those derived

from LiDAR, can be resampled or aggregated to a coarser spatial resolution and/or generalized using filters if desired. Resampling and aggregation decreases the number of cells that need to be processed, resulting in reduced computational time and costs, especially when predicting over large spatial extents. Higher spatial resolution may not be beneficial due to more local noise and detail that may hinder the modeling of more general patterns (Albani et al., 2004; Grohmann et al., 2011; Habib et al., 2018; McDermid and Franklin, 1994; Newman et al., 2018). In contrast, mapping or predicting smaller features on the landscape, such as sink holes (e.g., Ironside et al., 2018) or slope failures (e.g., Brock et al., 2020; Maxwell et al., 2020c, 2021), may require detailed, high spatial resolution data. The impact of spatial resolution and level of detail are likely problem specific; thus, if researchers have reason to believe that high spatial resolution is not necessary, does not merit the extra computational cost, and/or that reduced resolution may actually improve results, pilot studies should be implemented to systematically assess this sensitivity.

DLSM data used in studies and applied mapping or modeling projects should be fully described including collection methods and dates, original spatial resolution, and horizontal and vertical accuracies. If preprocessing is performed, such as resampling or aggregating, interpolation of contours or point clouds to generate raster surfaces, or local smoothing with filters, the entire processing chain should be clearly described and ideally scripted in an open-source, reproducible manner. To foster transparency and reproducibility, researchers should make source code, scripts, and/or input and output data available and include explanations and metadata.

4.1.3. Parameterizing moving windows and characterizing the landscape at varying scales

Configuring local moving windows —or window-like scales for various DLSM filtering approaches—can be complex due to the number of options available including window shape, window size, and cell weighting techniques. Prior studies may offer only limited guidance as noted by Ironside et al. (2018). Analysts should consider using larger window sizes to potentially reduce the impact of errors in the input DLSM and artifacts from the interpolation process. It is also important to consider the scale of the features of interest, as characterization of finer scale features or phenomena may require a small window size. Some prior authors have explored averaging calculations across multiple window sizes and/or including multiple versions of the input, calculated using different window sizes, in the feature space (e.g., Maxwell et al., 2016, 2020c, 2021; Maxwell and Warner, 2019a, 2019b). In the context of GEOBIA and segmentation of DTM data, Drăguţ et al. (2011) suggest a method to select appropriate scales using measures of local variance and spatial autocorrelation. We specifically recommend further exploration and adoption of the multi-scale landscape characterization methods proposed by Behrens et al. (2018a, 2018b) and implemented for predicting soil parameters. These methods are conceptually sound and allow for generation of intuitive land-surface parameters with reduced processing artifacts. We argue that there is a need for a standard method to be adopted to characterize multi-scale land-surface characteristics and that a movement away from traditional, window-based methods may be merited.

4.1.4. Generating DLSMs of difference

DLSMs of difference can be useful for mapping and quantifying landscape change resulting from natural processes (e.g., James et al., 2012; Perignon et al., 2013) or anthropogenic impacts (e.g., Maxwell and Strager, 2013; Ross et al., 2016). However, it is important to consider the impact of registration, co-registration, and elevation measurement errors in the resulting difference surfaces. Derived estimates of erosion and deposition (in the case of natural processes) or cut-and-fill (in the case of human disturbance) extents should make use of thresholds defined by the errors associated with the input DLSM data (Eq. (7) and Eq. (8)). Errors will be especially pronounced when differencing historic, photogrammetrically-derived surfaces or comparing them to more recent LiDAR or InSAR data. Error rates may not be consistent across the DLSMs due to the merging of multiple datasets or differences in land cover and/or terrain conditions. It is important to clearly document the accuracies of the input surfaces and the assumptions made when generating DLSMs of difference.

4.2. Research needs

4.2.1. Multi-scale land-surface characterization

As noted by Ironside et al. (2018), there is a need to further explore the impact of window shape, size, and cell weightings on calculated land-surface parameters and predictive models and offer guidance on appropriate parameterization. We argue that this is a major hinderance in effectively incorporating land-surface parameters into research and applied mapping and modeling tasks; further, this issue is especially daunting to those new to geomorphometry and DLSM analysis and processing. Given the large number of configuration options, we argue that it is currently not possible to generate a truly optimal set of multi-scale land-surface parameters. Thus, broader exploration and refinement of methods not reliant on traditional moving windows, such as those proposed by Behrens et al. (2018a, 2018b), should be a major research objective in geomorphometry, as this could greatly ease the creation and use of land-surface parameters across disciplines.

4.2.2. Model generalization

There is a need to explore how well feature spaces and models trained in a given landscape extrapolate or generalize to new regions with different geologic and climatic conditions and resulting physiographies. For example, Maxwell et al. (2021) quantified reductions in slope failure occurrence predictive model performance when models trained in different physiographic regions of West Virginia, USA were extrapolated to other regions within the state even though the most important features were fairly consistent. Lack of generalization is consistently an issue in developing models to apply to new datasets or landscapes, perhaps resulting from overfitting and differing landscape conditions, feature signatures, and spatial heterogeneity (James et al., 2013; Maxwell et al., 2018). This currently limits the utility of empirical modeling based on machine learning. Improving generalization is key to further operationalizing machine learning-based predictive modeling.

4.2.3. Deep learning

Given the large number of variables that can be calculated and the need for parameterization, modeling and mapping methods that require less feature space engineering (i.e., generating, preparing, selecting, and augmenting input variables) should be investigated. For example, deep learning methods that make use of convolutional neural networks (CNNs) may require a smaller subset of input land-surface parameters to obtain adequate results than traditional machine learning methods (Maxwell et al., 2020b; Zhang et al., 2016; Zhu et al., 2017). CNNs model patterns in data by learning weights associated with moving windows or kernels. This allows for the modeling of relationships or patterns in multiple dimensions including two-dimensional space, three-dimensional space, time, the spectral domain, elevation, and depth at a variety of scales. Such methods have recently led to rapid advances in computer vision and autonomous vehicle technologies (Hoeser et al., 2020; Hoeser and Kuenzer, 2020; Ma et al., 2019; Zhang et al., 2016; Zhu et al., 2017). Since the majority of local terrain measures rely on moving windows, it may be possible for CNNs to learn useful local patterns from a small set of terrain representations, such as HSs and SlpSs, as opposed to being provided a large feature space of pre-defined land-surface parameters. Based on our own visual interpretation of high spatial resolution DLSMs and derivatives for geologic, geohazard, and surficial geologic mapping, certain derivatives can offer key visual, textural, or contextual clues for mapping and delineation. Exploring how CNN-based deep learning may or may not mimic human

interpretation would be enlightening.

Researchers are beginning to explore the use of deep learning methods for geomorphic and landform mapping or the extraction of specific features. For example, Maxwell et al. (2020a) investigated the use of the Mask R-CNN (He et al., 2017) instance segmentation deep learning algorithm for extracting valley fill faces, geomorphic features resulting from mountaintop removal surface coal mining reclamation, using only a SlpS as input. They documented strong performance for extracting the extent of these features with some reduction in performance when applying the model to new geographic extents to assess generalization. Li et al. (2020) proposed a general framework for landform mapping using deep learning and noted improved performance in comparison to RF, a traditional machine learning method that does not incorporate convolutional operations to learn spatial patterns. Deep learning has also been explored for identifying features of archeological interest from digital terrain data (e.g., Guyot et al., 2021). These recent deep learning studies are building upon earlier landform mapping work relying on GEOBIA and segmentation techniques (e.g., Dragut, 2011; Drăguţ et al., 2011; Drăguţ and Blaschke, 2006; Drăguţ and Eisank, 2011; Gerçek et al., 2011; Pedersen, 2016; Verhagen and Drăguţ, 2012) and merit continued exploration. A key need is to explore the impact of feature space and terrain representations provided as predictor variables, the use of transfer learning techniques, in which models are initialized using weights learned from other datasets to potentially reduce overfitting and the need for large training datasets (Tan et al., 2018), the applications of unsupervised and semi-supervised techniques, and the development of data augmentation methods appropriate for digital terrain data. Research associated with specific CNN architectures, convolutional operations, and combining manual feature space engineering with CNN-based pattern recognition is also needed.

4.2.4. *Land-surface change detection*

Landscape and land cover change detection is a common application of multitemporal, remotely sensed imagery, such as multispectral imagery collected from satellite platforms with consistent return intervals (Lillesand et al., 2015). As discussed above, change detection of digital terrain surfaces has primarily relied on differencing DLSMs while taking into account the impact of error (Williams, 2012) to differentiate true change from error or noise. However, there is a need to explore other means of assessing, quantifying, or documenting landscape change, such as deep learning methods. Some prior studies have explored change using categorical representations of the landscape; for example, Maxwell and Strager (2013) assessed landscape change resulting from mountaintop removal surface coal mining by comparing landforms generated from pre- and post-mining DLSMs. There is a need to further explore change detection techniques relying on categorical representations such as geomorphons. GEOBIA and deep learning techniques for mapping or extracting landforms or specific landscape features need further research in the context of assessing and quantifying natural landscape change and anthropogenic landscape alterations.

5. Conclusions

Empirical predictive mapping and modeling rely on training data and predictor variables, which can include land-surface parameters derived from DLSMs. Our goal was to explore the use of digital elevation data and associated derivatives for use in empirical predictive models. If adequate DLSM data are available, a variety of spatially continuous parameters can be derived, many of which have been shown to be predictive of landscape processes and features of interest in ecology, geomorphology, vegetation mapping, geohazard prediction, and spatial probabilistic modeling in general. However, selecting features is complex due to the large number of potential parameters to choose from and the potential impacts of DLSM data source, spatial resolution, and level of detail and parameterization of moving windows or application of other methods to characterize the landscape at multiple scales. The existing literature may offer contradictory or incomplete guidance. The recommendations made here can be used to guide researchers and analysts in developing a feature space for specific mapping or modeling tasks. It is our hope that better characterization of the land surface using metrics that are predictive of the phenomena and/or features of interest will improve feature space design and ultimately boost model efficiency and performance.

Funding

This work was funded by the National Science Foundation (NSF) (Federal Award ID Number 2046059: "CAREER: Mapping Anthropocene Geomorphology with Deep Learning, Big Data Spatial Analytics, and LiDAR"). Additional funding was provided by a NASA West Virginia Space Grant Consortium research seed grant.

Declaration of Competing Interest

The authors declare no conflict of interest.

Acknowledgments

Thanks to the West Virginia GIS Technical Center for providing the DLSM data used and Dr. Timothy Warner for reviewing an early draft of the manuscript. We would like to thank the three anonymous reviewers whose suggestions strengthened the work.

References

Albani, M., Klinkenberg, B., Andison, D.W., Kimmins, J.P., 2004. The choice of window size in approximating topographic surfaces from Digital Elevation Models. Int. J. Geogr. Inf. Sci. 18, 577–593. https://doi.org/10.1080/13658810410001701987.

Andrews, D., Bucknam, R.C., 1987. Fitting degradation of shoreline scarps by a nonlinear diffusion model. J. Geophys. Res. 92, 12857–12867.

ArcGIS Pro help—ArcGIS Pro | Documentation, 2021 [WWW Document], URL. https://pro.arcgis.com/en/pro-app/2.7/help/main/welcome-to-the-arcgis-pro-app-help.htm (accessed 8.24.21).

Arundel, S.T., Phillips, L.A., Lowe, A.J., Bobinmyer, J., Mantey, K.S., Dunn, C.A., Constance, E.W., Usery, E.L., 2015. Preparing The National Map for the 3D Elevation Program – products, process and research. Cartogr. Geogr. Inf. Sci. 42, 40–53. https://doi.org/10.1080/15230406.2015.1057229.

ASTER Global Digital Elevation Map, 2021. WWW Document. https://asterweb.jpl.nasa.gov/gdem.asp (accessed 7.15.21).

Barnes, R., Callaghan, K.L., Wickert, A.D., 2020. Computing water flow through complex landscapes – Part 2: finding hierarchies in depressions and morphological segmentations. Earth Surf. Dynam. 8, 431–445. https://doi.org/10.5194/esurf-8-431-2020.

Barnes, R., Callaghan, K.L., Wickert, A.D., 2021. Computing water flow through complex landscapes – Part 3: Fill–Spill–Merge: flow routing in depression hierarchies. Earth Surf. Dynam. 9, 105–121. https://doi.org/10.5194/esurf-9-105-2021.

Behrens, T., Zhu, A.-X., Schmidt, K., Scholten, T., 2010. Multi-scale digital terrain analysis and feature selection for digital soil mapping. Geoderma 155, 175–185.

Behrens, T., Schmidt, K., MacMillan, R.A., Rossel, R.A.V., 2018. Multi-scale digital soil mapping with deep learning. Sci. Rep. 8, 1–9.

Bennie, J., Huntley, B., Wiltshire, A., Hill, M.O., Baxter, R., 2008. Slope, aspect and climate: spatially explicit and implicit models of topographic microclimate in chalk grassland. Ecol. Model. 216, 47–59. https://doi.org/10.1016/j.ecolmodel.2008.04.010.

Blaszczynski, J.S., 1997. Landform Characterization with Geographic Information Systems, p. 9.

Bogaart, P., Troch, P., 2006. Curvature distribution within hillslopes and catchments and its effect on the hydrological response. Hydrol. Earth Syst. Sci. 10, 925–936.

Böhner, J., Antonić, O., 2009. Chapter 8 land-surface parameters specific to topo-climatology. In: Hengl, T., Reuter, H.I. (Eds.), Developments in Soil Science, Geomorphometry. Elsevier, pp. 195–226. https://doi.org/10.1016/S0166-2481(08)00008-1.

Breiman, L., 2001. Random forests. Mach. Learn. 45, 5–32.

Brewer, C.A., 2005. Designing Better Maps. A Guide for GIS Users, p. 1.

Brock, J., Schratz, P., Petschko, H., Muenchow, J., Micu, M., Brenning, A., 2020. The performance of landslide susceptibility models critically depends on the quality of digital elevation models. Geomat. Nat. Hazards Risk 11, 1075–1092. https://doi.org/10.1080/19475705.2020.1776403.

Cai, J., Luo, J., Wang, S., Yang, S., 2018. Feature selection in machine learning: a new perspective. Neurocomputing 300, 70–79. https://doi.org/10.1016/j.neucom.2017.11.077.

Callaghan, K.L., Wickert, A.D., 2019. Computing water flow through complex landscapes – Part 1: incorporating depressions in flow routing using FlowFill. Earth Surf. Dynam. 7, 737–753. https://doi.org/10.5194/esurf-7-737-2019.
Cavalli, M., Goldin, B., Comiti, F., Brardinoni, F., Marchi, L., 2017. Assessment of erosion and deposition in steep mountain basins by differencing sequential digital terrain models. Geomorphology, Sediment Dynamics in Alpine Basins 291, 4–16. https://doi.org/10.1016/j.geomorph.2016.04.009.
Chandrashekar, G., Sahin, F., 2014. A survey on feature selection methods. In: Computers & Electrical Engineering, 40th-year Commemorative Issue, 40, pp. 16–28. https://doi.org/10.1016/j.compeleceng.2013.11.024.
Chang, K.-T., 2008. Introduction to geographic information systems (McGraw-Hill Boston).
Chea, H., Sharma, M., 2019. Residential segregation in hillside areas of Seoul, South Korea: a novel approach of geomorphons classification. Appl. Geogr. 108, 9–21. https://doi.org/10.1016/j.apgeog.2019.04.009.
Chen, Y.-C., Sung, Q., Cheng, K.-Y., 2003. Along-strike variations of morphotectonic features in the Western Foothills of Taiwan: tectonic implications based on stream-gradient and hypsometric analysis. Geomorphology 56, 109–137.
Clubb, F.J., Mudd, S.M., Milodowski, D.T., Hurst, M.D., Slater, L.J., 2014. Objective extraction of channel heads from high-resolution topographic data. Water Resour. Res. 50, 4283–4304.
Corcoran, J., Knight, J., Brisco, B., Kaya, S., Cull, A., Murnaghan, K., 2011. The integration of optical, topographic, and radar data for wetland mapping in northern Minnesota. Can. J. Remote. Sens. 37, 564–582. https://doi.org/10.5589/m11-067.
Croke, J., Todd, P., Thompson, C., Watson, F., Denham, R., Khanal, G., 2013. The use of multi temporal LiDAR to assess basin-scale erosion and deposition following the catastrophic January 2011 Lockyer flood, SE Queensland, Australia. Geomorphology 184, 111–126. https://doi.org/10.1016/j.geomorph.2012.11.023.
Csillik, O., Drăguţ, L., 2018. Towards a Global Geomorphometric Atlas Using Google Earth Engine, p. 4.
De Reu, J., Bourgeois, J., Bats, M., Zwertvaegher, A., Gelorini, V., De Smedt, P., Chu, W., Antrop, M., De Maeyer, P., Finke, P., Van Meirvenne, M., Verniers, J., Crombé, P., 2013. Application of the topographic position index to heterogeneous landscapes. Geomorphology 186, 39–49. https://doi.org/10.1016/j.geomorph.2012.12.015.
Debeer, D., Strobl, C., 2020. Conditional permutation importance revisited. BMC bioinformatics 21 (1), 1–30.
Dietrich, W.E., Reiss, R., Hsu, M.-L., Montgomery, D.R., 1995. A process-based model for colluvial soil depth and shallow landsliding using digital elevation data. Hydrol. Process. 9, 383–400.
Doctor, D.H., Young, J.A., 2013. An Evaluation of Automated GIS Tools for Delineating Karst Sinkholes and Closed Depressions From 1-meter Lidar-derived Digital Elevation Data.
Dornik, A., Cheţan, M.A., Drăguţ, L., Dicu, D.D., Iliuţă, A., 2022. Optimal scaling of predictors for digital mapping of soil properties. Geoderma 405, 115453.
Dragut, L., 2011. Automated classification of topography from SRTM data using object-based image analysis. Geomorphometry 2011, 113–116.
Drăguţ, L., Blaschke, T., 2006. Automated classification of landform elements using object-based image analysis. Geomorphology 81, 330–344. https://doi.org/10.1016/j.geomorph.2006.04.013.
Drăguţ, L., Eisank, C., 2011. Object representations at multiple scales from digital elevation models. Geomorphology 129, 183–189. https://doi.org/10.1016/j.geomorph.2011.03.003.
Drăguţ, L., Eisank, C., Strasser, T., 2011. Local variance for multi-scale analysis in geomorphometry. Geomorphology 130, 162–172. https://doi.org/10.1016/j.geomorph.2011.03.011.
Dunne, K., Cunningham, P., Azuaje, F., 2002. Solutions to instability problems with sequential wrapper-based approaches to feature selection. J. Machine Learn. Res. 1–22.
Dyer, J.M., 2019. A GIS-based water balance approach using a LiDAR-Derived DEM captures fine-scale vegetation patterns. Remote Sens. 11, 2385. https://doi.org/10.3390/rs11202385.
Ehsani, A.H., Quiel, F., 2008. Geomorphometric feature analysis using morphometric parameterization and artificial neural networks. Geomorphology 99, 1–12. https://doi.org/10.1016/j.geomorph.2007.10.002.
Eisank, C., Drăguţ, L., Blaschke, T., 2011. A generic procedure for semantics-oriented landform classification using object-based image analysis. Geomorphometry 2011, 125–128.
Evans, I.S., 1972. General geomorphometry, derivatives of altitude, and descriptive statistics. Spat. Anal. Geomorphol. 17–90.
Evans, J.S., 2020. spatialEco. https://github.com/jeffreyevans/spatialEco (Last accessed January 16, 2022).
Evans, J.S., 2021. GradientMetrics. https://github.com/jeffreyevans/GradientMetrics (Last accessed January 16, 2022).
Evans, J.S., Cushman, S.A., 2009. Gradient modeling of conifer species using random forests. Landsc. Ecol. 24, 673–683. https://doi.org/10.1007/s10980-009-9341-0.
Evans, I.S., Minár, J., 2011. A classification of geomorphometric variables. In: International Geomorphometry, pp. 105–108.
Evans, J.S., Murphy, M.A., 2015. Package 'rfUtilities' R package 1, p. 1.
F.R.S, 1901. LIII. On lines and planes of closest fit to systems of points in space. Lond. Edinburgh Dublin Philos. Magaz. J. Sci. 2, 559–572. https://doi.org/10.1080/14786440109462720.
Farr, T.G., Rosen, P.A., Caro, E., Crippen, R., Duren, R., Hensley, S., Kobrick, M., Paller, M., Rodriguez, E., Roth, L., Seal, D., Shaffer, S., Shimada, J., Umland, J., Werner, M., Oskin, M., Burbank, D., Alsdorf, D., 2007. The shuttle radar topography mission. Rev. Geophys. 45, RG2004 https://doi.org/10.1029/2005RG000183.
Florinsky, I.V., 2017. An illustrated introduction to general geomorphometry. Progr. Phys. Geogr. 41, 723–752. https://doi.org/10.1177/0309133317733667.
Florinsky, I.V., Eilers, R.G., Manning, G.R., Fuller, L.G., 2002. Prediction of soil properties by digital terrain modelling. Environ. Model Softw. 17, 295–311. https://doi.org/10.1016/S1364-8152(01)00067-6.
Franklin, S.E., 1987. Geomorphometric processing of digital elevation models. Comput. Geosci. 13, 603–609. https://doi.org/10.1016/0098-3004(87)90030-6.
Franklin, S.E., 2020. Interpretation and use of geomorphometry in remote sensing: a guide and review of integrated applications. Int. J. Remote Sens. 41, 7700–7733. https://doi.org/10.1080/01431161.2020.1792577.
Friedman, J.H., 2001. Greedy function approximation: a gradient boosting machine. Ann. Stat. 1189–1232.
Fu, P., Rich, P.M., 2002. A geometric solar radiation model with applications in agriculture and forestry. Comput. Electron. Agric. 37, 25–35.
Gabet, E.J., Mudd, S.M., Wood, R., Grieve, S.W.D., Binnie, S.A., Dunai, T.J., 2021. Hilltop curvature increases with the square root of erosion rate. J. Geophys. Res. 126 (e2020JF005858).
Gallardo-Cruz, J.A., Pérez-García, E.A., Meave, J.A., 2009. β-Diversity and vegetation structure as influenced by slope aspect and altitude in a seasonally dry tropical landscape. Landsc. Ecol. 24, 473–482.
Georganos, S., Grippa, T., Vanhuysse, S., Lennert, M., Shimoni, M., Kalogirou, S., Wolff, E., 2018. Less is more: Optimizing classification performance through feature selection in a very-high-resolution remote sensing object-based urban application. GISci. Remote Sens. 55, 221–242.
Gerçek, D., Toprak, V., Strobl, J., 2011. Object-based classification of landforms based on their local geometry and geomorphometric context. Int. J. Geogr. Inf. Sci. 25, 1011–1023. https://doi.org/10.1080/13658816.2011.558845.
Gesseler, P.E., Moore, I.D., McKenzie, N.J., Ryan, P.J., 1995. Soil-landscape modelling and spatial prediction of soil attributes. Int. J. Geogr. Inf. Syst. 9, 421–432. https://doi.org/10.1080/02693799508902047.
Gessler, P.E., Moore, I., McKenzie, N.J., Ryan, P., 1995. Soil-landscape modelling and spatial prediction of soil attributes. Int. J. Geogr. Inf. Syst. 9, 421–432.
Goetz, J.N., Guthrie, R.H., Brenning, A., 2011. Integrating physical and empirical landslide susceptibility models using generalized additive models. Geomorphology 129, 376–386.
Goetz, J., Brenning, A., Petschko, H., Leopold, P., 2015. Evaluating machine learning and statistical prediction techniques for landslide susceptibility modeling. Comput. Geosci. 81, 1–11.
Goldberg, D.E., 2006. Genetic algorithms. Pearson Education India.
Grohmann, C.H., Smith, M.J., Riccomini, C., 2011. Multiscale analysis of topographic surface roughness in the Midland Valley, Scotland. IEEE Trans. Geosci. Remote Sens. 49, 1200–1213. https://doi.org/10.1109/TGRS.2010.2053546.
Gruber, S., Peckham, S., 2009. Chapter 7 land-surface parameters and objects in hydrology. In: Hengl, T., Reuter, H.I. (Eds.), Developments in Soil Science, Geomorphometry. Elsevier, pp. 171–194. https://doi.org/10.1016/S0166-2481(08)00007-X.
Guth, P.L., 2006. Geomorphometry from SRTM. Photogram. Eng. Remote Sens. 72, 269–277. https://doi.org/10.14358/PERS.72.3.269.
Guth, P., 2009. Chapter 15 geomorphometry in MicroDEM. In: Hengl, T., Reuter, H.I. (Eds.), Developments in Soil Science, Geomorphometry. Elsevier, pp. 351–366. https://doi.org/10.1016/S0166-2481(08)00015-9.
Guyon, I., Elisseeff, A., 2003. An introduction to variable and feature selection. J. Mach. Learn. Res. 3, 1157–1182.
Guyot, A., Lennon, M., Lorho, T., Hubert-Moy, L., 2021. Combined detection and segmentation of archeological structures from LiDAR data using a deep learning approach. J. Comput. Appl. Archaeol. 4, 1.
Habib, A., Khoshelham, K., Akdim, N., El Ghandour, F., Labbassi, K., Menenti, M., 2018. Impact of spatial resolution, interpolation and filtering algorithms on DEM accuracy for geomorphometric research: a case study from Sahel-Doukkala, Morocco. Model. Earth Syst. Environ. 4, 1537–1554. https://doi.org/10.1007/s40808-018-0512-3.
Hall-Beyer, M., 2017. Practical guidelines for choosing GLCM textures to use in landscape classification tasks over a range of moderate spatial scales. Int. J. Remote Sens. 38, 1312–1338. https://doi.org/10.1080/01431161.2016.1278314.
Haralick, R.M., Shanmugam, K., Dinstein, I.H., 1973. Textural features for image classification. IEEE Trans. Syst. Man Cybernet. 610–621.
He, K., Gkioxari, G., Dollár, P., Girshick, R., 2017. Mask r-cnn. In: Proceedings of the IEEE International Conference on Computer Vision, pp. 2961–2969.
Heerdegen, R.G., Beran, M.A., 1982. Quantifying source areas through land surface curvature and shape. J. Hydrol. 57, 359–373.
Heimsath, A.M., Dietrich, W.E., Nishiizumi, K., Finkel, R.C., 1997. The soil production function and landscape equilibrium. Nature 388, 358–361.
Hengl, T., Reuter, H.I., 2008. Geomorphometry: concepts, software, applications. Newnes.
Geomorphometry: concepts, software, applications. In: Hengl, T., Reuter, H.I., Institute for Environment and Sustainability (European Commission. Joint Research Centre) (Eds.), 2009. Developments in Soil Science, 1st ed. Elsevier, Amsterdam, Netherlands ; Oxford, UK ; Boston [Mass.].
Hoeser, T., Kuenzer, C., 2020. Object detection and image segmentation with deep learning on earth observation data: a review-part I: evolution and recent trends. Remote Sens. 12, 1667.
Hoeser, T., Bachofer, F., Kuenzer, C., 2020. Object detection and image segmentation with deep learning on earth observation data: a review—part II: applications. Remote Sens. 12, 3053. https://doi.org/10.3390/rs12183053.
Hofierka, J., Mitášová, H., Neteler, M., 2009. Chapter 17 geomorphometry in GRASS GIS. In: Hengl, T., Reuter, H.I. (Eds.), Developments in Soil Science, Geomorphometry. Elsevier, pp. 387–410. https://doi.org/10.1016/S0166-2481(08)00017-2.

Höfle, B., Rutzinger, M., 2011. Topographic airborne LiDAR in geomorphology: a technological perspective. Zeit fur Geo Supp 55, 1–29. https://doi.org/10.1127/0372-8854/2011/0055S2-0043.
Hooshyar, M., Wang, D., 2016. An analytical solution of Richards' equation providing the physical basis of SCS curve number method and its proportionality relationship. Water Resour. Res. 52, 6611–6620.
Howard, H.H., McMaster, R.B., Slocum, T.A., Kessler, F.C., 2008. Thematic Cartography and Geovisualization.
Hu, G., Dai, W., Li, S., Xiong, L., Tang, G., Strobl, J., 2021a. Quantification of terrain plan concavity and convexity using aspect vectors from digital elevation models. Geomorphology 375, 107553.
Hu, G., Wang, C., Li, S., Dai, W., Xiong, L., Tang, G., Strobl, J., 2021b. Using vertices of a triangular irregular network to calculate slope and aspect. Int. J. Geogr. Inform. Sci. 1–23.
Hughes, G., 1968. On the mean accuracy of statistical pattern recognizers. IEEE Trans. Inf. Theory 14, 55–63.
Hurst, M.D., Mudd, S.M., Walcott, R., Attal, M., Yoo, K., 2012. Using hilltop curvature to derive the spatial distribution of erosion rates. J. Geophys. Res. 117.
Hurst, R., Rollema, H., Bertrand, D., 2013. Nicotinic acetylcholine receptors: from basic science to therapeutics. Pharmacol. Ther. 137, 22–54.
Hyvärinen, A., Oja, E., 2000. Independent component analysis: algorithms and applications. Neural Networks 13, 411–430.
Ironside, K.E., Mattson, D.J., Arundel, T., Theimer, T., Holton, B., Peters, M., Edwards Jr, T.C., Hansen, J., 2018. Geomorphometry in Landscape Ecology: Issues of scale, physiography, and application. Environment and Ecology Research 6 (5), 397–412.
James, L.A., Hodgson, M.E., Ghoshal, S., Latiolais, M.M., 2012. Geomorphic change detection using historic maps and DEM differencing: the temporal dimension of geospatial analysis. In: Geomorphology, Geospatial Technologies and Geomorphological Mapping Proceedings of the 41st Annual Binghamton Geomorphology Symposium, 137, pp. 181–198. https://doi.org/10.1016/j.geomorph.2010.10.039.
James, G., Witten, D., Hastie, T., Tibshirani, R., 2013. An Introduction to Statistical Learning. Springer.
Jasiewicz, J., Stepinski, T.F., 2013. Geomorphons — a pattern recognition approach to classification and mapping of landforms. Geomorphology 182, 147–156. https://doi.org/10.1016/j.geomorph.2012.11.005.
Jasiewicz, J., Netzel, P., Stepinski, T.F., 2013. Content-based landscape retrieval using geomorphons. Geomorphometry 2013, 52–54.
Jenness, J.S., 2004. Calculating landscape surface area from digital elevation models. Wildl. Soc. Bull. 32, 829–839.
Johnstone, S.A., Hudson, A.M., Nicovich, S., Ruleman, C.A., Sare, R.M., Thompson, R.A., 2018. Establishing chronologies for alluvial-fan sequences with analysis of high-resolution topographic data: San Luis Valley, Colorado, USA. Geosphere 14, 2487–2504.
Kai, L., Guo'an, T., Sheng, J., 2013. Research on the classification of terrain texture from DEMs based on BP neural network. Geomorphometry 2013, 1–4.
Kalousis, A., Prados, J. and Hilario, M., 2005, November. Stability of feature selection algorithms. In Fifth IEEE International Conference on Data Mining (ICDM'05) (pp. 8-pp). IEEE.
Kennedy, J., Eberhart, R., 1995. Particle swarm optimization. In: Proceedings of ICNN'95-International Conference on Neural Networks. IEEE, pp. 1942–1948.
Khalid, S., Khalil, T., Nasreen, S., 2014. A survey of feature selection and feature extraction techniques in machine learning. In: 2014 Science and Information Conference, pp. 372–378. https://doi.org/10.1109/SAI.2014.6918213.
Kienzle, S., 2004. The effect of DEM raster resolution on first order, second order and compound terrain derivatives. Trans. GIS 8, 83–111. https://doi.org/10.1111/j.1467-9671.2004.00169.x.
Kirby, E., Whipple, K.X., 2012. Expression of active tectonics in erosional landscapes. J. Struct. Geol. 44, 54–75.
Knight, J.F., Tolcser, B.P., Corcoran, J.M., Rampi, L.P., 2013. The effects of data selection and thematic detail on the accuracy of high spatial resolution wetland classifications. Photogramm. Eng. Remote Sens. 79, 613–623.
Kreslavsky, M.A., Head, J.W., Neumann, G.A., Rosenburg, M.A., Aharonson, O., Smith, D.E., Zuber, M.T., 2013. Lunar topographic roughness maps from Lunar Orbiter Laser Altimeter (LOLA) data: scale dependence and correlation with geologic features and units. Icarus 226, 52–66.
Kuhn, M., Wickham, H., 2020. Tidymodels: A Collection of Packages for Modeling and Machine Learning Using Tidyverse Principles.
Kuhn, M., Wickham, H., 2021. recipes: Preprocessing Tools to Create Design Matrices.
Kumari, N., Saco, P.M., Rodriguez, J.F., Johnstone, S.A., Srivastava, A., Chun, K.P., Yetemen, O., 2020. The grass is not always greener on the other side: seasonal reversal of vegetation greenness in aspect-driven semiarid ecosystems. Geophys. Res. Lett. 47 (e2020GL088918).
Lague, D., Davy, P., 2003. Constraints on the long-term colluvial erosion law by analyzing slope-area relationships at various tectonic uplift rates in the Siwaliks Hills (Nepal). J. Geophys. Res. 108.
Lague, D., Crave, A., Davy, P., 2003. Laboratory experiments simulating the geomorphic response to tectonic uplift. J. Geophys. Res. 108 (ETG-3).
LaHusen, S.R., Duvall, A.R., Booth, A.M., Montgomery, D.R., 2016. Surface roughness dating of long-runout landslides near Oso, Washington (USA), reveals persistent postglacial hillslope instability. Geology 44, 111–114.
Langston, A.L., Tucker, G.E., Anderson, R.S., Anderson, S.P., 2015. Evidence for climatic and hillslope-aspect controls on vadose zone hydrology and implications for saprolite weathering. Earth Surf. Process. Landf. 40, 1254–1269.
Law, M.H., Figueiredo, M.A., Jain, A.K., 2004. Simultaneous feature selection and clustering using mixture models. IEEE transactions on pattern analysis and machine intelligence 26 (9), 1154–1166.
Lecours, V., Devillers, R., Simms, A.E., Lucieer, V.L., Brown, C.J., 2017. Towards a framework for terrain attribute selection in environmental studies. Environ. Model Softw. 89, 19–30.
Li, X., Hodgson, M.E., 2004. Vector field data model and operations. GISci. Remote Sens. 41, 1–24.
Li, S., Xiong, L., Tang, G., Strobl, J., 2020. Deep learning-based approach for landform classification from integrated data sources of digital elevation model and imagery. Geomorphology 354, 107045.
Libohova, Z., Winzeler, H.E., Lee, B., Schoeneberger, P.J., Datta, J., Owens, P.R., 2016. Geomorphons: landform and property predictions in a glacial moraine in Indiana landscapes. CATENA 142, 66–76. https://doi.org/10.1016/j.catena.2016.01.002.
Lifton, N.A., Chase, C.G., 1992. Tectonic, climatic and lithologic influences on landscape fractal dimension and hypsometry: implications for landscape evolution in the San Gabriel Mountains, California. Geomorphology 5, 77–114.
Lillesand, T., Kiefer, R.W., Chipman, J., 2015. Remote Sensing and Image Interpretation. John Wiley & Sons.
Lopez, M., Berry, J.K., 2002. Use surface area for realistic calculations. GeoWorld 15, 25.
Lundberg, S.M., Lee, S.-I., 2017. A unified approach to interpreting model predictions. In: Proceedings of the 31st International Conference on Neural Information Processing Systems, pp. 4768–4777.
Lundberg, S.M., Erion, G., Chen, H., DeGrave, A., Prutkin, J.M., Nair, B., Katz, R., Himmelfarb, J., Bansal, N., Lee, S.-I., 2019. Explainable AI for Trees: From Local Explanations to Global Understanding (arXiv preprint arXiv:1905.04610).
Lyew-Ayee, P., Viles, H.A., Tucker, G.E., 2007. The use of GIS-based digital morphometric techniques in the study of cockpit karst. Earth Surf. Process. Landf. 32, 165–179. https://doi.org/10.1002/esp.1399.
Ma, L., Liu, Y., Zhang, X., Ye, Y., Yin, G., Johnson, B.A., 2019. Deep learning in remote sensing applications: a meta-analysis and review. ISPRS J. Photogramm. Remote Sens. 152, 166–177.
MacMillan, R.A., Shary, P.A., 2009. Chapter 9 landforms and landform elements in geomorphometry. In: Hengl, T., Reuter, H.I. (Eds.), Developments in Soil Science, Geomorphometry. Elsevier, pp. 227–254. https://doi.org/10.1016/S0166-2481(08)00009-3.
Mather, J.R., 1978. The Climatic Water Budget in Environmental Analysis (Write Source Generation III).
Maxwell, A.E., Strager, M.P., 2013. Assessing Landform Alterations Induced by Mountaintop Mining 2013. https://doi.org/10.4236/ns.2013.52A034.
Maxwell, Aaron E., Warner, T.A., 2019a. Is high spatial resolution DEM data necessary for mapping palustrine wetlands? Int. J. Remote Sens. 40, 118–137. https://doi.org/10.1080/01431161.2018.1506184.
Maxwell, Aaron E., Warner, T.A., 2019b. Is high spatial resolution DEM data necessary for mapping palustrine wetlands? Int. J. Remote Sens. 40, 118–137.
Maxwell, A.E., Warner, T.A., Strager, M.P., 2016. Predicting palustrine wetland probability using random forest machine learning and digital elevation data-derived terrain variables. Photogram. Eng. Remote Sens. 82, 437–447. https://doi.org/10.14358/PERS.82.6.437.
Maxwell, A.E., Warner, T.A., Fang, F., 2018. Implementation of machine-learning classification in remote sensing: an applied review. Int. J. Remote Sens. 39, 2784–2817. https://doi.org/10.1080/01431161.2018.1433343.
Maxwell, A.E., Bester, M.S., Guillen, L.A., Ramezan, C.A., Carpinello, D.J., Fan, Y., Hartley, F.M., Maynard, S.M., Pyron, J.L., 2020a. Semantic segmentation deep learning for extracting surface mine extents from historic topographic maps. Remote Sens. 12, 4145. https://doi.org/10.3390/rs12244145.
Maxwell, A.E., Pourmohammadi, P., Poyner, J.D., 2020b. Mapping the topographic features of mining-related valley fills using mask R-CNN deep learning and digital elevation data. Remote Sens. 12, 547. https://doi.org/10.3390/rs12030547.
Maxwell, A.E., Sharma, M., Kite, J.S., Donaldson, K.A., Thompson, J.A., Bell, M.L., Maynard, S.M., 2020c. Slope failure prediction using random forest machine learning and LiDAR in an eroded folded mountain belt. Remote Sens. 12, 486. https://doi.org/10.3390/rs12030486.
Maxwell, A.E., Sharma, M., Kite, J.S., Donaldson, K.A., Maynard, S.M., Malay, C.M., 2021. Assessing the generalization of machine learning-based slope failure prediction to new geographic extents. ISPRS Int. J. Geo Inf. 10, 293. https://doi.org/10.3390/ijgi10050293.
McCune, B., Keon, D., 2002. Equations for potential annual direct incident radiation and heat load. J. Veg. Sci. 13, 603–606. https://doi.org/10.1111/j.1654-1103.2002.tb02087.x.
McDermid, G.J., Franklin, S.E., 1994. Spectral, spatial, and geomorphometric variables for the remote sensing of slope processes. Remote Sens. Environ. 49, 57–71. https://doi.org/10.1016/0034-4257(94)90059-0.
McKean, J., Roering, J., 2004. Objective landslide detection and surface morphology mapping using high-resolution airborne laser altimetry. Geomorphology 57, 331–351. https://doi.org/10.1016/S0169-555X(03)00164-8.
Milodowski, D., Mudd, S., Mitchard, E., 2015. Topographic roughness as a signature of the emergence of bedrock in eroding landscapes. Earth Surf. Dynam. 3, 483–499.
Minár, J., Jenčo, M., Evans Jr., I.S., Kadlec, M., Krcho, J., Pacina, J., Burian, L., Benová, A., 2013. Third-order geomorphometric variables (derivatives): definition, computation and utilization of changes of curvatures. Int. J. Geogr. Inf. Sci. 27, 1381–1402. https://doi.org/10.1080/13658816.2013.792113.
Minár, J., Evans, I.S., Jenčo, M., 2020. A comprehensive system of definitions of land surface (topographic) curvatures, with implications for their application in geoscience modelling and prediction. Earth Sci. Rev., 103414

Montgomery, D.R., Dietrich, W.E., 1992. Channel initiation and the problem of landscape scale. Science 255, 826–830.
Montgomery, D.R., Foufoula-Georgiou, E., 1993. Channel network source representation using digital elevation models. Water Resour. Res. 29, 3925–3934.
Moodie, A.J., Pazzaglia, F.J., Berti, C., 2018. Exogenic forcing and autogenic processes on continental divide location and mobility. Basin Res. 30, 344–369. https://doi.org/10.1111/bre.12256.
Moore, I., Lewis, A., Gallant, J., 1993. Terrain Attributes: Estimation Methods and Scale Effects.
Murphy, M.A., Evans, J.S., Storfer, A., 2010. Quantifying Bufo boreas connectivity in Yellowstone National Park with landscape genetics. Ecology 91, 252–261.
Newman, D.R., Lindsay, J.B., Cockburn, J.M.H., 2018. Evaluating metrics of local topographic position for multiscale geomorphometric analysis. Geomorphology 312, 40–50. https://doi.org/10.1016/j.geomorph.2018.04.003.
Nori, H., Jenkins, S., Koch, P., Caruana, R., 2019. Interpretml: A Unified Framework for Machine Learning Interpretability (arXiv preprint arXiv:1909.09223).
Olaya, V., Conrad, O., 2009. Chapter 12 geomorphometry in SAGA. In: Hengl, T., Reuter, H.I. (Eds.), Developments in Soil Science, Geomorphometry. Elsevier, pp. 293–308. https://doi.org/10.1016/S0166-2481(08)00012-3.
Passalacqua, P., Trung, T.D., Foufoula-Georgiou, E., Sapiro, G., Dietrich, W.E., 2010. A geometric framework for channel network extraction from lidar: nonlinear diffusion and geodesic paths. J. Geophys. Res. 115. https://doi.org/10.1029/2009JF001254.
Pedersen, G.B.M., 2016. Semi-automatic classification of glaciovolcanic landforms: an object-based mapping approach based on geomorphometry. J. Volcanol. Geotherm. Res. 311, 29–40. https://doi.org/10.1016/j.jvolgeores.2015.12.015.
Pelletier, J.D., 2013. A robust, two-parameter method for the extraction of drainage networks from high-resolution digital elevation models (DEMs): evaluation using synthetic and real-world DEMs. Water Resour. Res. 49, 75–89. https://doi.org/10.1029/2012WR012452.
Pelletier, J.D., Barron-Gafford, G.A., Gutiérrez-Jurado, H., Hinckley, E.-L.S., Istanbulluoglu, E., McGuire, L.A., Niu, G.-Y., Poulos, M.J., Rasmussen, C., Richardson, P., et al., 2018. Which way do you lean? Using slope aspect variations to understand Critical Zone processes and feedbacks. Earth Surf. Process. Landf. 43, 1133–1154.
Perignon, M.C., Tucker, G.E., Griffin, E.R., Friedman, J.M., 2013. Effects of riparian vegetation on topographic change during a large flood event, Rio Puerco, New Mexico, USA. J. Geophys. Res. 118, 1193–1209. https://doi.org/10.1002/jgrf.20073.
Perron, J.T., Royden, L., 2013. An integral approach to bedrock river profile analysis. Earth Surf. Process. Landf. 38, 570–576.
Pike, R.J., Wilson, S.E., 1971. Elevation-relief ratio, hypsometric integral, and geomorphic area-altitude analysis. Geol. Soc. Am. Bull. 82, 1079–1084.
Pike, R.J., Evans, I.S., Hengl, T., 2009. Chapter 1 geomorphometry: a brief guide. In: Hengl, Tomislav, Reuter, H.I. (Eds.), Developments in Soil Science, Geomorphometry. Elsevier, pp. 3–30. https://doi.org/10.1016/S0166-2481(08)00001-9.
Purinton, B., Bookhagen, B., 2017. Validation of digital elevation models (DEMs) and comparison of geomorphic metrics on the southern Central Andean Plateau. Earth Surf. Dynam. 5, 211–237.
R Core Team, 2020. R: A Language and Environment for Statistical Computing. R Foundation for Statistical Computing, Vienna, Austria.
Rampi, L.P., Knight, J.F., Pelletier, K.C., 2014. Wetland mapping in the upper midwest United States. Photogramm. Eng. Remote Sens. 80, 439–448.
Reed, M., Kite, S., 2020. Peripheral gully and landslide erosion on an extreme anthropogenic landscape produced by mountaintop removal coal mining. Earth Surf. Process. Landf. 45, 2078–2090.
Reuter, H.I., Hengl, T., Gessler, P., Soille, P., 2009. Chapter 4 preparation of DEMs for geomorphometric analysis. In: Hengl, Tomislav, Reuter, Hannes, I. (Eds.), Developments in Soil Science, Geomorphometry. Elsevier, pp. 87–120. https://doi.org/10.1016/S0166-2481(08)00004-4.
Rich, P., Dubayah, R., Hetrick, W., Saving, S., 1994. Using viewshed models to calculate intercepted solar radiation: applications in ecology. In: American Society for Photogrammetry and Remote Sensing Technical Papers. American Society of Photogrammetry and Remote Sensing, pp. 524–529.
Riley, S.J., DeGloria, S.D., Elliot, R., 1999. Index that quantifies topographic heterogeneity. Intermount. J. Sci. 5, 23–27.
Riley, J.W., Calhoun, D.L., Barichivich, W.J., Walls, S.C., 2017. Identifying small depressional wetlands and using a topographic position index to infer hydroperiod regimes for pond-breeding amphibians. Wetlands 37, 325–338. https://doi.org/10.1007/s13157-016-0872-2.
Roberts, D.W., Cooper, S.V., 1989. Concepts and techniques of vegetation mapping. In: Land Classifications Based on Vegetation: Applications for Resource Management, pp. 90–96.
Roering, J.J., Kirchner, J.W., Dietrich, W.E., 1999. Evidence for nonlinear, diffusive sediment transport on hillslopes and implications for landscape morphology. Water Resour. Res. 35, 853–870.
Roering, J.J., Mackey, B.H., Marshall, J.A., Sweeney, K.E., Deligne, N.I., Booth, A.M., Handwerger, A.L., Cerovski-Darriau, C., 2013. 'You are HERE': connecting the dots with airborne lidar for geomorphic fieldwork. Geomorphology 200, 172–183.
Ross, M.R.V., McGlynn, B.L., Bernhardt, E.S., 2016. Deep impact: effects of mountaintop mining on surface topography, bedrock structure, and downstream waters. Environ. Sci. Technol. 50, 2064–2074. https://doi.org/10.1021/acs.est.5b04532.
Sangireddy, H., Stark, C.P., Kladzyk, A., Passalacqua, P., 2016. GeoNet: an open source software for the automatic and objective extraction of channel heads, channel network, and channel morphology from high resolution topography data. Environ. Model Softw. 83, 58–73. https://doi.org/10.1016/j.envsoft.2016.04.026.
Sărășan, A., Józsa, E., Ardelean, A.C., Drăguț, L., 2019. Sensitivity of geomorphons to mapping specific landforms from a digital elevation model: a case study of drumlins. Area 51, 257–267. https://doi.org/10.1111/area.12451.
Serneels, S., De Nolf, E., Van Espen, P.J., 2006. Spatial sign preprocessing: a simple way to impart moderate robustness to multivariate estimators. J. Chem. Inf. Model. 46, 1402–1409.
Silva, V., Tenenbaum, J., 2002. Global versus local methods in nonlinear dimensionality reduction. Adv. Neural Inf. Proces. Syst. 15.
Sofia, G., 2020. Combining geomorphometry, feature extraction techniques and Earth-surface processes research: the way forward. Geomorphology 355, 107055.
Stage, A.R., 1976. An expression for the effect of aspect, slope, and habitat type on tree growth. For. Sci. 22, 457–460.
Stanley, T., Kirschbaum, D.B., 2017. A heuristic approach to global landslide susceptibility mapping. Nat. Hazards 87, 145–164.
Stepinski, T.F., Jasiewicz, J., 2011. Geomorphons-a new approach to classification of landforms. Proceedings of geomorphometry 109–112.
Strobl, C., Boulesteix, A.-L., Zeileis, A., Hothorn, T., 2007. Bias in random forest variable importance measures: illustrations, sources and a solution. BMC Bioinformatics 8, 1–21.
Strobl, C., Boulesteix, A.-L., Kneib, T., Augustin, T., Zeileis, A., 2008. Conditional variable importance for random forests. BMC Bioinformatics 9, 1–11.
Strobl, C., Hothorn, T., Zeileis, A., 2009. Party on!.
Struble, W.T., Roering, J.J., 2021. Hilltop curvature as a proxy for erosion rate: wavelets enable rapid computation and reveal systematic underestimation. Earth Surf. Dynam. Discuss. 1–35.
Struble, W.T., Roering, J.J., Dorsey, R.J., Bendick, R., 2021. Characteristic scales of drainage reorganization in Cascadia. Geophys. Res. Lett. 48 https://doi.org/10.1029/2020GL091413 e2020GL091413.
Tan, C., Sun, F., Kong, T., Zhang, W., Yang, C., Liu, C., 2018. A survey on deep transfer learning. In: International Conference on Artificial Neural Networks. Springer, pp. 270–279.
Tarboton, D.G., 1997. A new method for the determination of flow directions and upslope areas in grid digital elevation models. Water Resour. Res. 33, 309–319.
Tarboton, D.G., 2005. Terrain Analysis Using Digital Elevation Models (TauDEM), 3012. Utah State University, Logan, p. 2018.
Tarboton, D., Liu, Y., Sazib, N.S., Wang, S., 2016. Accelerating TauDEM for extracting hydrology information from national-scale high resolution topographic dataset. In: Proceedings of the XSEDE16 Conference on Diversity, Big Data, and Science at Scale, pp. 1–2.
Tarolli, P., Sofia, G., Dalla Fontana, G., 2012. Geomorphic features extraction from high-resolution topography: landslide crowns and bank erosion. Nat. Hazards 61, 65–83.
Thaler, E.A., Larsen, I.J., Yu, Q., 2021. The extent of soil loss across the US Corn Belt. Proc. Natl. Acad. Sci. 118.
Tucker, G.E., Bras, R.L., 1998. Hillslope processes, drainage density, and landscape morphology. Water Resour. Res. 34, 2751–2764.
Tucker, G.E., Hancock, G.R., 2010. Modeling landscape evolution. Earth Surf. Process. Landf. 35 (1), 28–50.
Turc, L., 1961. Evaluation des besoins en eau d'irrigation, évapotranspiration potentielle. Ann. Agron. 12, 13–49.
Turowski, J.M., Cook, K.L., 2017. Field techniques for measuring bedrock erosion and denudation. Earth Surf. Process. Landf. 42, 109–127.
Qin, C., Zhu, A.X., Pei, T., Li, B., Zhou, C., Yang, L., 2007. An adaptive approach to selecting a flow-partition exponent for a multiple-flow-direction algorithm. International Journal of Geographical Information Science 21 (4), 443–458.
Verhagen, P., Drăguț, L., 2012. Object-based landform delineation and classification from DEMs for archaeological predictive mapping. J. Archaeol. Sci. 39, 698–703. https://doi.org/10.1016/j.jas.2011.11.001.
Vermeulen, D., Van Niekerk, A., 2017. Machine learning performance for predicting soil salinity using different combinations of geomorphometric covariates. Geoderma 299, 1–12. https://doi.org/10.1016/j.geoderma.2017.03.013.
Warner, T., 2011. Kernel-based texture in remote sensing image classification. Geogr. Compass 5, 781–798. https://doi.org/10.1111/j.1749-8198.2011.00451.x.
Wegmann, K.W., Zurek, B.D., Regalla, C.A., Bilardello, D., Wollenberg, J.L., Kopczynski, S.E., Ziemann, J.M., Haight, S.L., Apgar, J.D., Zhao, C., Pazzaglia, F.J., 2007. Position of the Snake River watershed divide as an indicator of geodynamic processes in the greater Yellowstone region, western North America. Geosphere 3, 272–281. https://doi.org/10.1130/GES00083.1.
Willgoose, G., Bras, R.L., Rodriguez-Iturbe, I., 1991. A physical explanation of an observed link area-slope relationship. Water Resour. Res. 27, 1697–1702.
Williams, R., 2012. DEMs of Difference. Geomorphological Techniques, p. 2.
Wilson, J.P., Gallant, J.C., 2000. Terrain Analysis: Principles and Applications. John Wiley & Sons.
Wilson, M.F., O'Connell, B., Brown, C., Guinan, J.C., Grehan, A.J., 2007. Multiscale terrain analysis of multibeam bathymetry data for habitat mapping on the continental slope. Mar. Geod. 30, 3–35.
Wood, J., 1996. The Geomorphological Characterisation of Digital Elevation Models. University of Leicester, United Kingdom.
Wood, J., 2009. Chapter 14 geomorphometry in LandSerf. In: Hengl, T., Reuter, H.I. (Eds.), Developments in Soil Science, Geomorphometry. Elsevier, pp. 333–349. https://doi.org/10.1016/S0166-2481(08)00014-7.
Wright, C., Gallant, A., 2007. Improved wetland remote sensing in Yellowstone National Park using classification trees to combine TM imagery and ancillary environmental data. Remote Sens. Environ. 107, 582–605. https://doi.org/10.1016/j.rse.2006.10.019.

Xiong, L., Guoan, T., Yang, X., Fayuan, F., 2021. Geomorphology-oriented digital terrain anlaysis: progress and perspectives. J. Geogr. Sci. 31 (3), 456–476. https://doi.org/10.1007/s11442-021-1853-9.

Yang, C.-J., Turowski, J.M., Hovius, N., Lin, J.-C., Chang, K.-J., 2021. Badland landscape response to individual geomorphic events. Nat. Commun. 12, 1–8.

Zar, J.H., 1972. Significance testing of the Spearman rank correlation coefficient. J. Am. Stat. Assoc. 67, 578–580.

Zevenbergen, L.W., Thorne, C.R., 1987. Quantitative analysis of land surface topography. Earth Surf. Process. Landf. 12, 47–56.

Zhang, Liangpei, Zhang, Lefei, Du, B., 2016. Deep learning for remote sensing data: a technical tutorial on the state of the art. IEEE Geosci. Remote Sens. Magazine 4, 22–40.

Zhao, H., Fang, X., Ding, H., Josef, S., Xiong, L., Na, J., Tang, G., 2017. Extraction of terraces on the loess plateau from high-resolution DEMs and imagery utilizing object-based image analysis. ISPRS Int. J. Geo Inf. 6, 157. https://doi.org/10.3390/ijgi6060157.

Zhu, X.X., Tuia, D., Mou, L., Xia, G.-S., Zhang, L., Xu, F., Fraundorfer, F., 2017. Deep learning in remote sensing: a comprehensive review and list of resources. IEEE Geosci. Remote Sens. Magazine 5, 8–36.